Rivista Italiana di Paleontologia e Stratigrafia
(*Research in Paleontology and Stratigraphy*)
vol. 131(2): 353-381. **July 2025**
DOI: https://doi.org/10.54103/2039-4942/27969

LATE BERRIASIAN–EARLY VALANGINIAN EVOLUTION AND DROWNING OF THE GETIC CARBONATE PLATFORM (SE SERBIA)

JELENA STEFANOVIĆ[1*], GIOVANNA DELLA PORTA[2], IOAN I. BUCUR[3,4] & DEJAN RADIVOJEVIĆ[1]

[1]University of Belgrade, Faculty of Mining and Geology, Department for Regional Geology, Belgrade, Serbia.
E-mail: jelena.stefanovic@rgf.bg.ac.rs; dejan.radivojevic@rgf.bg.ac.rs
[2]Università degli Studi di Milano, Dipartimento di Scienze della Terra, via Mangiagalli 34 - 20133 Milano - Italia.
E-mail: giovanna.dellaporta@unimi.it
[3]Babeş-Bolyai University, Department of Geology and Centre for Integrated Geological Studies, Cluj-Napoca, Romania.
E-mail: ioan.bucur@ubbcluj.ro
[4]Romanian Academy, Cluj Branch, Republicii str. 9, 400015, Cluj-Napoca, Romania.
*Corresponding author.

Associate Editor: Luca Martire

To cite this article: Stefanović J., Della Porta G., Bucur I.I. & Radivojević D. (2025) - Late Berriasian-early Valanginian evolution and drowning of the Getic Carbonate Platform (SE Serbia). *Rivista Italiana di Paleontologia e Stratigrafia*, vol. 131(2): 353-381.

Keywords: microfacies; carbon and oxygen stable isotopes; Early Cretaceous; Carpatho-Balkanides.

Abstract: The Early Cretaceous was a time of significant development of carbonate platforms on the margins of the Tethys Ocean, including the Getic Carbonate Platform, in the northern peri-Tethys realm, cropping out in the Southern Carpathians (Romania) and Carpatho-Balkanides (Serbia and Bulgaria). This study focusses on the upper Berriasian–lower Valanginian carbonate succession of SE Serbia (Dimitrovgrad) and provides noteworthy insights for the understanding of the Getic Carbonate Platform evolution. On the basis of facies stacking pattern and occurrence of prominent horizons, three vertically superimposed sedimentary units are distinguished in the ~230 m thick succession: unit I consists of shallow subtidal, low-energy environments favouring the development of patch reefs with *Bacinella-Lithocodium*, rudists, corals, siliceous and calcareous sponges, including stromatoporoids; unit II is indicative of restricted subtidal to intertidal-supratidal facies and platform-top subaerial exposure, testified by karst collapse breccias, syn-sedimentary dolomitization and by negative shifts of carbon and oxygen isotopes; unit III represents the platform drowning stage with abundance of crinoids, chert, detrital quartz and glaucony grains. Platform drowning is marked by a change in carbonate production from photozoan, light-dependent skeletal biota such as corals, to light-independent, filter feeders heterozoan carbonates with crinoids and bryozoans. Syn-sedimentary tectonics appears to be responsible for uplift and subaerial exposure, subsequent rapid deepening and platform demise, possibly associated with increased nutrients during transgression. The Berriasian–Valanginian carbonate strata of Dimitrovgrad show similar evolution to other contemporaneous carbonate systems of western Tethys, highlighting the effects of regional tectonics and global controlling factors on carbonate deposition in the earliest Cretaceous.

Received: January 11, 2025; accepted: May 21, 2025

Introduction

Extensive carbonate depositional systems developed across the northern to southern provinces of the Tethyan Realm from the Late Jurassic to the Early Cretaceous (Dercourt et al. 2000; Kiessling et al. 2003; Höfling & Scott 2002). These shallow-water carbonate successions recorded Jurassic to Cretaceous global changes driven by climate variations, tectonics and eustatic sea-level oscillations (Hallam 1985; Frakes et al. 1992; Larson and Erba 1999; Weissert and Erba 2004; Immenhauser et al. 2005; Föllmi 2012; Haq 2014; Cavalheiro et al. 2021; Martinez et al. 2023). The Berriasian–Valanginian time is regarded as one of the most dynamic intervals of the Early Cretaceous, affected by a perturbation of the global carbon cycle (Weissert et al. 1998), associated with the first Oceanic Anoxic Event (OAE) of the Cretaceous period ("Weissert OAE"; Erba et al. 2004). During the Berriasian–Valanginian time, carbonate platforms in different paleogeographic domains of the Tethys Ocean, from the northern passive margin Helvetic platform and intra-Tethys Northern Calcareous Alps, reveal the following stages of evolution: a) pre-drowning shallow-water carbonate platform growth; b) subaerial exposure of the platform top in some areas (Masse et al. 2009; Grădinaru et al. 2016); and c) carbonate platform drowning (Föllmi et al. 1994; Schlagintweit & Ebli 1999; Föllmi et al. 2006, 2007; Morales et al. 2013). Various studies (Morales et al. 2013; Föllmi & Godet 2013) described a change in carbonate production from photozoan association, dominated by benthic, light-dependent organisms and non-skeletal grains, to heterozoan association, dominated by light-independent organisms (sensu James 1997), corresponding to the tropical shallow-water and cool-water carbonate factories, respectively (sensu Schlager 2000, 2003).

The drowning of carbonate platforms was defined by Schlager (1981) as the demise of shallow-water carbonate production due to rapid accommodation creation (e.g., rapid tectonic or eustatic deepening or sedimentation rate reduction) or suffocation by siliciclastic input and/or seawater eutrophication reducing the carbonate factory capability to keep pace with increasing accommodation. The sedimentary expression of drowning events often consists of hemipelagic deposits sharply covering shallow-water carbonates (Schlager 1981, 1989, 1999ab; Schlager & Camber 1986). Drowning events may follow the subaerial exposure of carbonate platforms, commonly manifested by karstification and/or calcrete paleosoil formation, because exposure switches off the carbonate factory and then, at the onset of the following relative sea-level rise, drastically reduces the carbonate production rates by a lag time (Schlager 1989; Hillgärtner 1998; Gawlick & Schlagintweit 2006; Merino-Tomé et al. 2012; Godet et al. 2013 and references therein).

The goal of this study is to investigate the lowermost Cretaceous carbonate succession cropping out in south-eastern Serbia (Dimitrovgrad area; Fig. 1), belonging to the complex system of carbonate platforms, labelled by Patrulius (1976) and Patrulius and Avram (1976) as the Getic Carbonate Platform (GCP), to identify the stages of platform evolution in comparison with other Tethyan domains. Present-day outcrops of the GCP extend from the Southern Carpathians (Romania) to their southern continuation in the Carpatho-Balkanides (Serbia and Bulgaria). Following several studies in the Romanian (cf. Grădinaru et al. 2016; Pleş et al. 2019, Mircescu et al. 2022) and Bulgarian (Ivanova et al. 2008; Ivanova & Chatalov 2022) sectors of the GCP, this study aims at characterizing the carbonate facies and microfacies, the skeletal composition of bioconstructions and the response of the SE Serbian portion of the Lower Cretaceous GCP to the regional tectonics and global perturbation driving subaerial exposure, platform drowning and carbonate factory changes.

Geological setting

The Upper Jurassic–Lower Cretaceous carbonates of the GCP belong to the Getic Nappe (Fig. 1) that formed during the Late Cretaceous, as a result of the two-phase collision between the Dacia Mega-Unit and the stable part of the European continent, the Moesian Platform (Săndulescu 1984; Schmid et al. 2008, 2020; Krstekanić et al. 2020). The GCP carbonate succession was deposited on the European-derived Dacia Mega-Unit (Fig. 2; Csontos & Vörös 2004; Schmid et al. 2008).

In Serbia and Bulgaria, different local names are in use to address the Upper Jurassic–Lower Cretaceous GCP outcrops (Kräutner & Krstić 2003). For instance, in the study area in SE Serbia, Upper

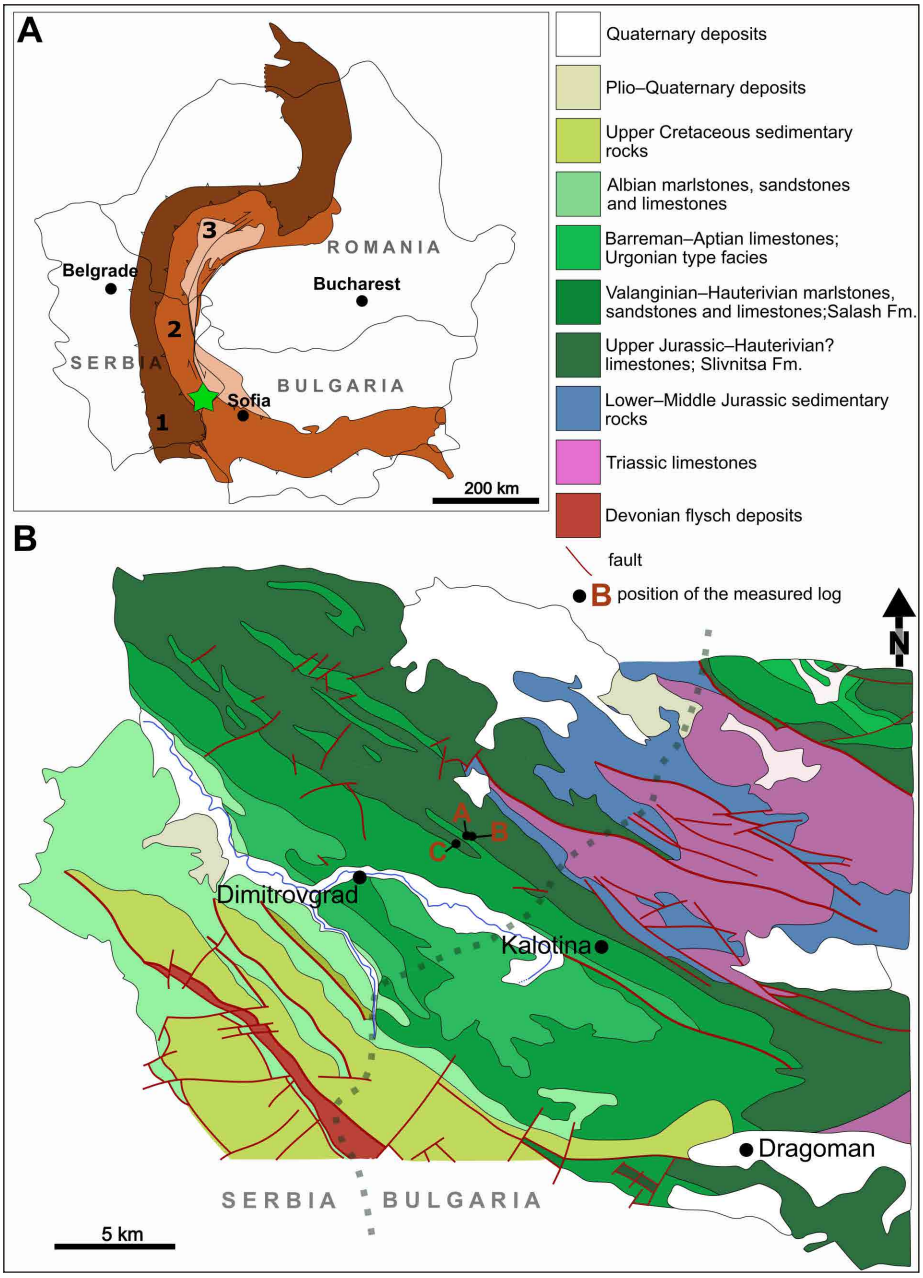

Fig. 1 - A) Location of the investigated area in SE Serbia within the Carpatho-Balkanides. Numbers represent the thrust sheets forming the orogen: (1) Serbo-Macedonian-Supragetic-Subbucovinian-Bucovinian, (2) Getic and (3) Danubian nappes (modified and simplified after Schmid et al. 2008). The green star represents the investigated area near the town of Dimitrovgrad. B) Detail of the geological map of SE Serbia, in the area of Dimitrovgrad (redrafted after the Basic Geological Map of Yugoslavia, 1:100,000 Sheet Pirot and Breznik, Anđelković et al. 1975) and western Bulgaria, in the proximity of Dragoman and Kalotina (redrafted after Geological Map of the Republic of Bulgaria, 1:50,000 Dragoman Map Sheet, Angelov et al. 2010).

Jurassic to Lower Cretaceous carbonate platform successions are labelled as part of the Kučaj and Tupižnica-Teposh zones (cf. Dimitrijević 1997), or in western Bulgaria they are addressed as part of the Dragoman positive block (Sapunov et al. 1985; Ivanova et al. 2008). Hence, the definition of GCP is accepted herein for all Upper Jurassic–Lower Cretaceous carbonate successions forming the sedimentary cover of the Getic Nappe, specifically comprising the Serbian and Bulgarian segments, to be able to compare the carbonate deposits across different regions and define significant regional events recorded in other parts of the complex GCP sedimentary system.

Previous studies on the Lower Cretaceous Getic Carbonate Platform

This study focuses on outcrops located in the surroundings of the town of Dimitrovgrad, representing the south-eastern part of the Serbian GCP, which continues into western Bulgaria. Publications on the uppermost Jurassic–lowermost Cretaceous carbonate strata of SE Serbia are limited, except for studies dealing with the paleontological characterization and biostratigraphy based on calcareous algae (Radoičić 1978; Bucur et al. 2021) and benthic foraminifera (Bucur et al. 1995; Bubík et al. 2024).

The Serbian part of the GCP was initially investigated by Anđelković et al. (1969) in the Basic

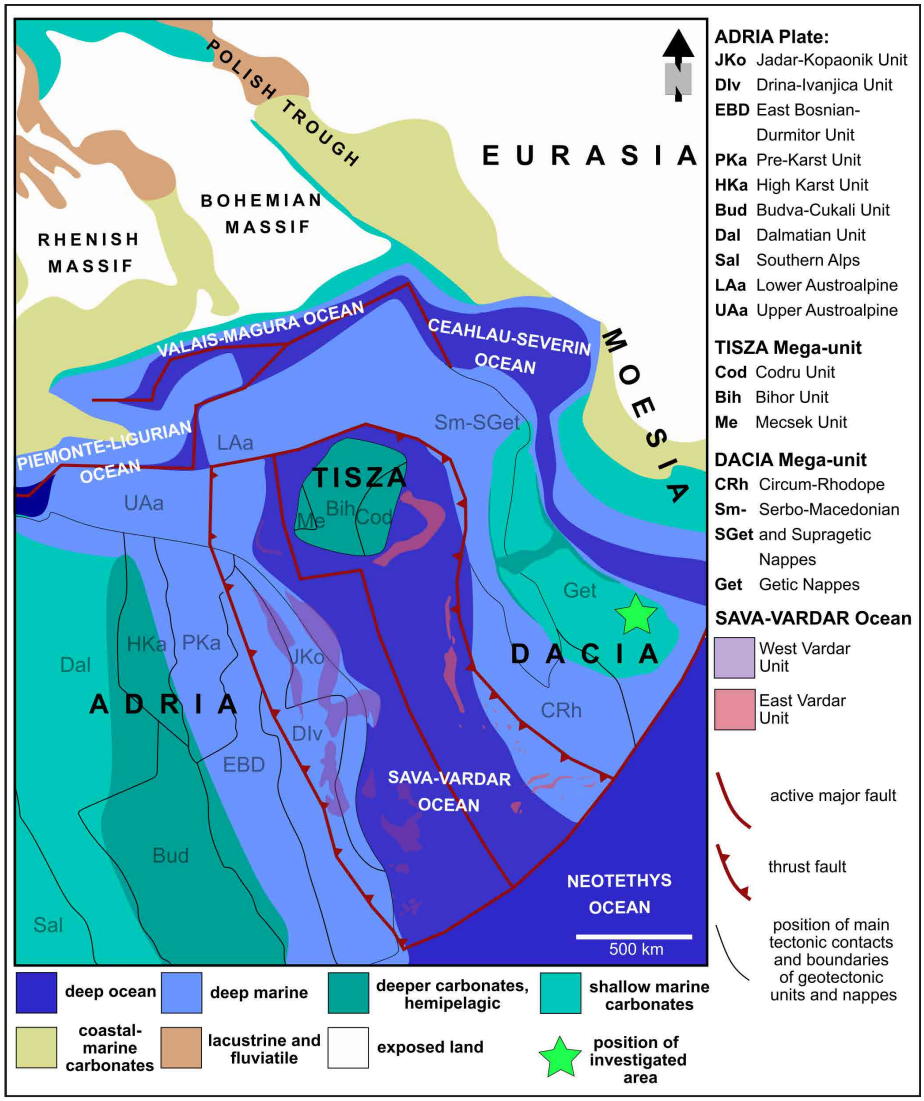

Fig. 2 - Paleogeographic map of the portion of the Tethyan Realm including future Dinarides, Alps, Western, Eastern and Southern Carpathians, during earliest Cretaceous, modified after Dercourt et al. (2000). The position of the main geotectonic units was defined based on van Hinsbergen et al. (2020). The approximate position of the investigated area is marked by the green star, and according to Dercourt et al. (2000) Getic Zone during the Early Cretaceous was positioned around the 25° N palaeolatitude (cf. Bucur et al. 1995).

Geological Map of SFRY (1:100,000), Sheet Pirot and Breznik (Fig. 1), and partially by Jankičević (1978). The sedimentological composition of the lowermost Cretaceous carbonates was locally investigated in the southern part of the Serbian GCP (Bucur et al. 1995) and in its south-western segment (Bucur et al. 2020).

In the Bulgarian sector, named Dragoman Block, two different formations were recognized in the Jurassic to Lower Cretaceous sedimentary succession of the GCP, with variable diachronous boundaries (Ivanova et al. 2000; Ivanova & Koleva-Rekalova 2004; Roniewicz 2008; Ivanova et al. 2008; Petrova et al. 2017; Kołodziej & Ivanova 2021; Ivanova & Chatalov 2022): 1) Callovian–lower Hauterivian shallow marine limestones of the Slivnitsa Formation, and 2) Berriasian–Barremian open marine marlstones, sandstones and limestones of the Salash Formation. These studies show that the lithological contact between the shallow-water carbonates of Slivnitsa Fm., and marly limestones and marlstones of the Salash Fm., becomes younger westward, starting in late early Valanginian in the easternmost part and up to the latest Valanginian–early Hauterivian in the western part of the Dragoman Block. In addition, the boundary between these two formations can be transitional (Ivanova et al. 2000) or represented by a hardground (Mandov & Nikolov 2001). Recently, Ivanova & Chatalov (2022) investigated the Valanginian drowning event capping the Slivnitsa Fm. carbonates.

Materials and methods

Three stratigraphic logs were measured and correlated in the selected study area close to the town of Dimitrovgrad: log A (110 m thick; latitude

N 43° 01' 45", longitude E 22° 49' 09"), log B (200 m thick; latitude N 43° 01' 40", longitude E 22° 49' 23") and log C (70 m thick; latitude N 43° 01' 37", longitude E 22° 48' 48"). A total number of 75 samples was collected from which 83 thin sections were prepared for petrographic analysis. The standard classification of carbonate rock depositional textures by Dunham (1962), integrated with Embry & Klovan (1971), was used for the description of carbonate facies and microfacies. Staining of thin sections with alizarine red was performed for the identification of dolomite (Dickson 1965, 1966).

The classification by Védrine et al. (2007) was applied to identify the types of oncoids. This classification is based on surface morphology, size, cortex structure and composition and distinguishes four categories of oncoids (type 1–4). Type 1 oncoids are homogenous or made of continuous, but barely visible, micritic laminae. Type 2 oncoids exhibit dominance of micritic laminae over the organism-bearing laminations made of serpulid worms or polymorphinid foraminifera *Bullopora* Quenstedt, 1856. Both, type 1 and 2, have a bioclastic or lithoclastic nucleus (Védrine et al. 2007). Type 3 oncoids are few millimetres to 5 cm in diameter, elliptical bodies with lobate surface. The cortex is dominantly composed of organism-bearing laminae of microencrusters *Bacinella irregularis* Radoičić, 1959 and *Lithocodium aggregatum* Elliott 1956, followed by few micritic laminations. Both types of laminae are rarely continuous. Type 4 oncoids show no lamination in the cortex and no nucleus and are made of microbial meshwork of *Bacinella* and *Lithocodium*. The classification by Strasser (1986) was used to characterize the ooids.

The age of the studied succession was determined on the basis of benthic foraminifera and calcareous nannoplankton associations.

Stable oxygen and carbon isotope analyses were conducted on carbonate powders extracted by handheld microdrill. Sampling for chemostratigraphy covered the entire stratigraphic section but at unequal distances. The extraction of total 78 powders was performed separating the depositional texture from veins and fractures filled by late diagenetic calcite. The analysed samples include: 68 bulk rock (log A: 24 samples; log B: 28 samples; log C: 15 limestone samples, 1 dolomite sample) and 10 calcite spar cement from fractures and veins crosscutting the lithified limestone. Fracture filling sparite was sampled to constrain the isotopic signature of late burial diagenesis that might have overprinted the pristine marine carbonate isotopic values. Stable isotope analysis was performed at the Department of Earth Sciences, University of Milan, using an automated carbonate preparation device (Gasbench II) and a Thermo Fisher Scientific Delta V Advantage continuous flow mass spectrometer. Carbonate powder samples were reacted with > 99% orthophosphoric acid at 70°C. The carbon and oxygen isotope compositions are expressed in the conventional delta notation calibrated to the Vienna Pee-Dee Belemnite (V-PDB) scale by the international standards IAEA 603, NBS-18 and internal laboratory Carrara and Candoglia marble standards calibrated against V-PDB. Analytical reproducibility for these analyses was better than ± 0.1 ‰ for both $\delta^{18}O$ and $\delta^{13}C$ values. A two-point moving average was calculated to identify vertical trends and isotope excursions through time and for chemostratigraphic correlation of logs.

Scanning electron microscopy analysis was performed with a JEOL JSM-6610LV equipped with an energy-dispersive X-ray spectrometer (SEM-EDX) on selected samples at the University of Belgrade, Faculty of Mining and Geology, Laboratory of SEM. The prepared polished rock samples were exposed to the EDX analyses, while obtaining secondary electron and back-scattered images.

Results

Sedimentary units and facies characterization

Detailed sedimentological and petrographic investigation of logs A, B and C, allowed distinguishing 17 facies types, labelled from F1 to F17, complemented by microfacies petrographic descriptions of thin sections as described in detail in Table 1. Three superimposed stratigraphic intervals, labelled as unit I, II and III (Fig. 3), were distinguished on the basis of facies character, sharp lithological changes (e.g., occurrence of F14 sponge spicule packstone with chert) and horizons of lithoclastic breccia beds (facies F7a-b).

Unit I consists of facies from F1 to F6, with different vertical distribution in the lower parts of the three logs: in log A facies F1-F3, F5, F6 (43 m thick); in log B F1, F2, F4, F5 (163 m thick); and in log C F2, F3 (17 m thick). Facies F1 consists of 0.5-2 m-thick beds of peloidal packstone/grainstone to

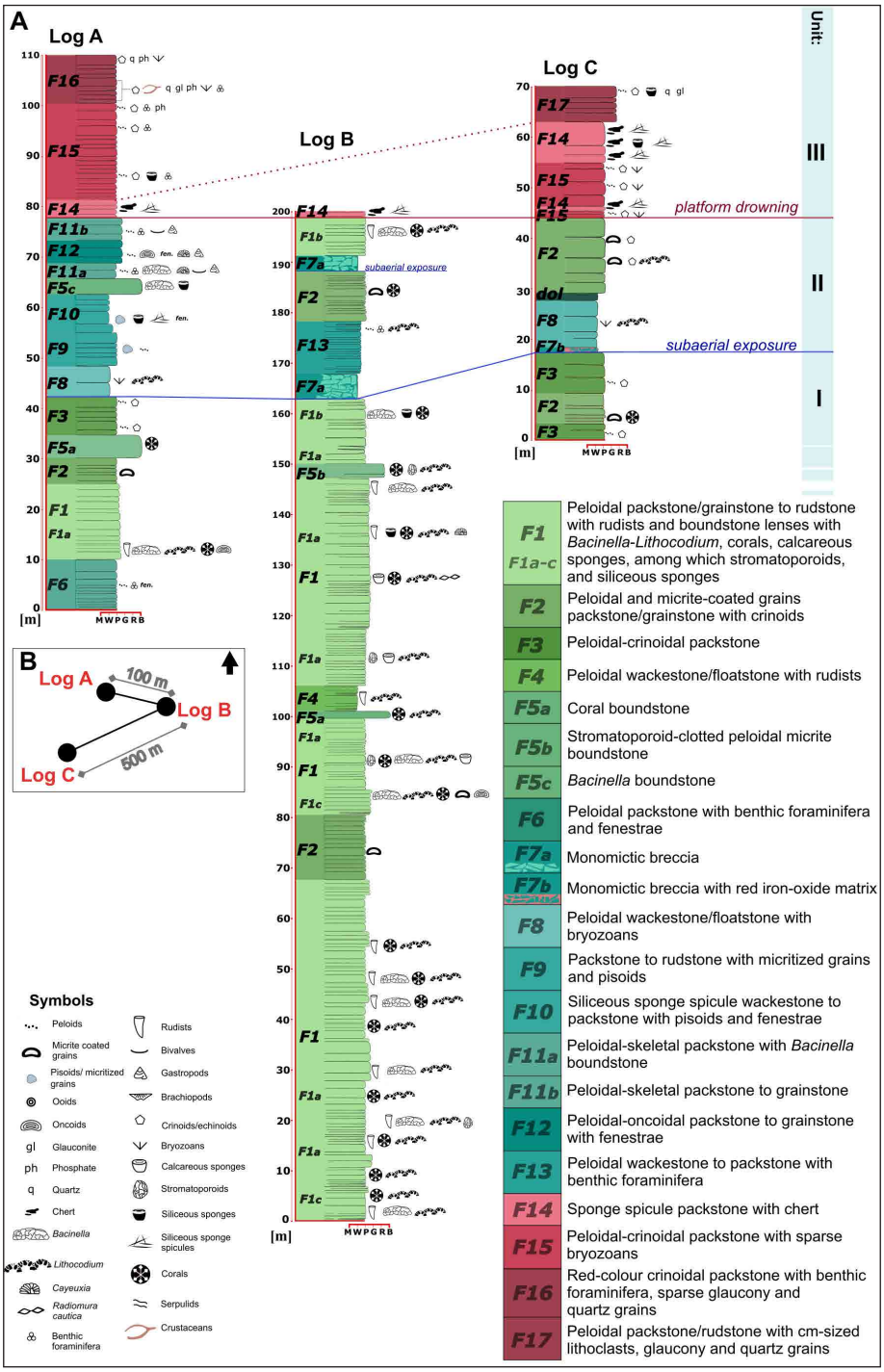

Fig. 3 - A) Sedimentary logs A, B and C measured in the Dimitrovgrad area. Seventeen facies and microfacies types were identified and three superimposed stratigraphic units (I-III) were distinguished from bottom to top (unit I-III). B) Relative position of logs with the relative distance in metres (not to scale).

rudstone with rudists, surrounding decimetre-scale lenses of boundstone with *Bacinella-Lithocodium*, corals, calcareous sponges, among which stromatoporoids, and siliceous sponges (Fig. 4). Three subcategories of facies F1 were distinguished on the basis of dominant biota in the boundstone lenses: F1a is dominated by corals (Fig. 5A), calcareous and siliceous sponges (Fig. 5B-C); F1b shows dominant rudists and *Bacinella-Lithocodium*; and F1c is characterized by stromatoporoids. Some of the skeletal components, such as rudist shells, stromatoporoids and corals, are encrusted by *Bacinella-Lithocodium* (Fig. 5D) and locally by foraminifera (Fig. 5E). *Bacinella* and *Lithocodium* may exhibit perforations by the foraminifer *Troglotella incrustans* Wernli & Fookes, 1992 (Fig. 5F) as reviewed by Schlagintweit (2012). These microproblematica organisms also form 1-4 mm wide, type 3 and 4 oncoids. Two subtypes of type 4 oncoids are differentiated in this study: *Bacinella*-dominated oncoids, which are sub-rounded to ellip-

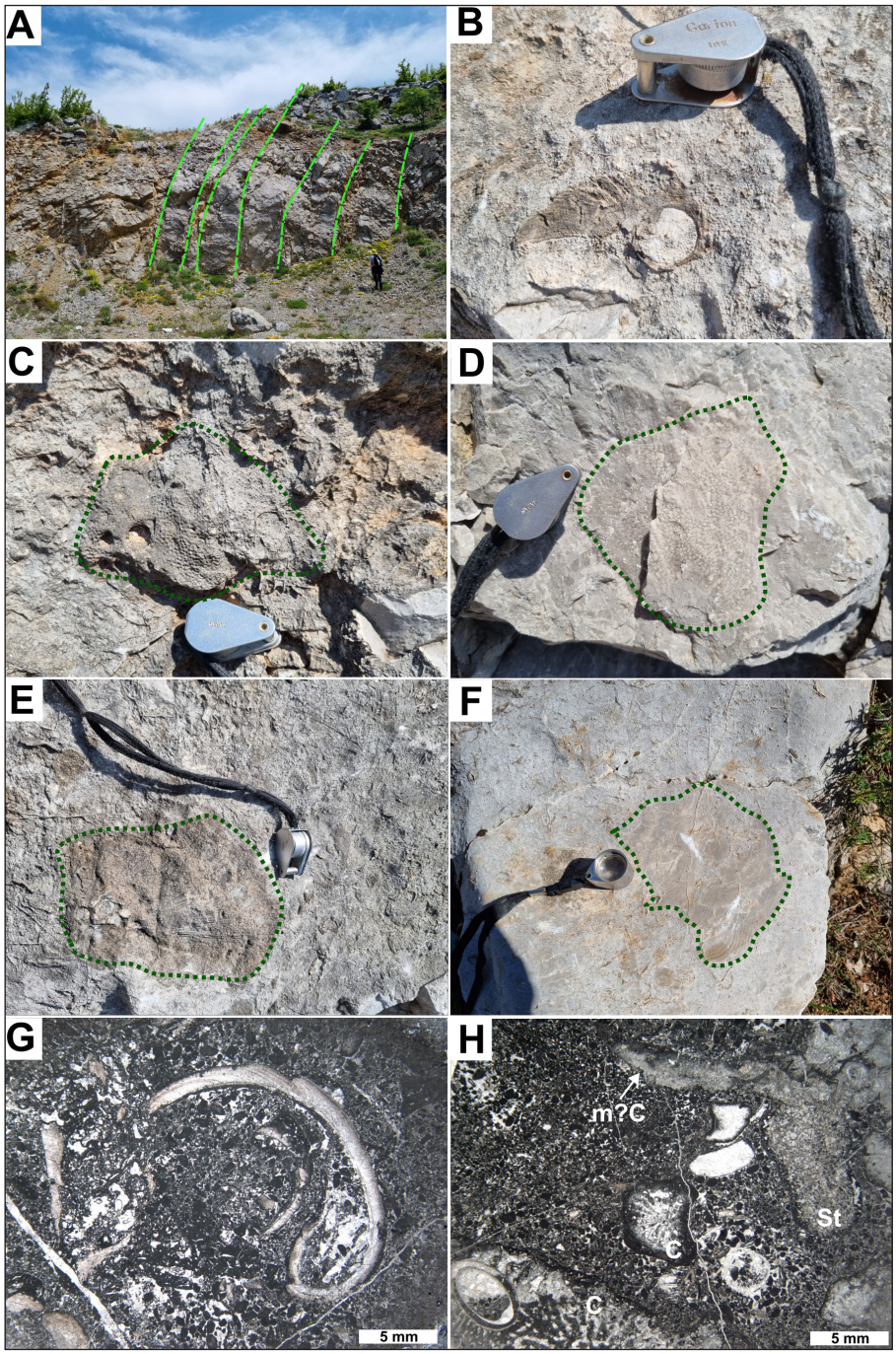

Fig. 4 - Outcrop photos and photomicrographs of facies F1 (unit I, logs A and B). A) Tectonically tilted 0.5-2 m thick beds of F1 peloidal packstone/grainstone to rudstone showing bedding, with different boundstone lenses with corals, calcareous sponges, among which stromatoporoids, siliceous sponges, rudists and *Bacinella-Lithocodium* (unit I, log B). B) Outcrop photo of centimetre-size rudists (log B). C) Decimetre-size unidentified sponge with borings (log B). D-F) Decimetre-size stromatoporoids (log B). G) Peloidal packstone/grainstone to rudstone surrounding dm-scale lenses of boundstone with rudists (sample A0, log B). H) Peloidal packstone/grainstone to rudstone surrounding dm-scale lenses of boundstone with stromatoporoids (St) and corals (coral = C; meandroid? coral = m?C). Note the boring on the coral (C) with geopetal filling (sample 101/12, log A).

tical, occasionally with thin *Lithocodium* coating (Fig. 5G); and *Lithocodium*-dominated oncoids, which have wavy edges, are elongated and *Bacinella* is rare to absent (Fig. 5H). Facies F2 peloidal and micrite-coated grains packstone/grainstone with crinoids (Fig. 6A-B) contains type 4 *Lithocodium*-dominated oncoids and locally rims of fibrous isopachous cement (Fig. 6C). Facies F3 well-sorted, peloidal-crinoidal packstone is dominated by crinoid ossicle debris (Fig. 6D). Facies F4 peloidal wackestone/floatstone with rudist fragments is rich in silt-grade skeletal debris embedding few, coarse skeletal grains (Fig. 6E), and it is crossed by irregular millimetre-wide fissures with intraclasts, peloids and micrite matrix (Fig. 6F). Beds of F5a boundstone (Fig. 7A) occur in log B (~100 m) represented by cerioid corals, and in log A (~35 m), where plocoid corals are encrusted by serpulids (Fig. 7B). In log A, fissures with red colour, siliciclastic sediment with iron oxides and calcite cement cross-cut the F5a boundstone (Fig. 7B). Based on the EDX analyses the red deposits consist of iron oxides, muscovite and other detrital mica grains, rutile and clay minerals (sample 101/10; Appendix 1). Boundstone beds with stro-

Facies	Texture	Sorting and grain size	Grain types	Skeletal grains	Bedding	Diagenetic features	Depositional environment
F1– Peloidal packstone/grainstone to rudstone with rudists and boundstone lenses with* Bacinella-Lithocodium*, corals, calcareous sponges, among which stromatoporoids, and siliceous sponges ***F1a – Peloidal P/G to R with corals and sponges*** ***F1b – Peloidal P/G to R with rudists and* Bacinella-Lithocodium** ***F1c – Peloidal P/G to R with stromatoporoids***	P/G to R	Poorly sorted, locally moderate sorted; 0.04- > 6 mm.	Peloids (90-600 µm, commonly 200-300 µm) (A); micrite coated grains (0.5-1.5 mm) (S-C); oncoids type 3 and 4 made of *Bacinella* and *Lithocodium*, with skeletal fragments of rudists, sponges and nubecularid foraminifera (1-4 mm) (VR-C); skeletal grains (0.6-10 mm, occasionally >20 mm) (A)	Rudists (VC), probably Family Requieniidae and/or Monopleuridae; bivalves (VR); gastropods (VR); crinoids (C); echinoid spines (R); siliceous demosponges with monoaxone spicules (S); calcified sponge *Cylicopsis verticalis* and other undetermined calcareous sponges (S); stromatoporoids (R-VC); solitary corals (R-C); cerioid (R-C); fabello-meandroid? and meandroid (S); plocoid corals (R); *Bacinella-Lithocodium* encrusting rudists, corals, stromatoporoids and other sponges (C); *Crescentiella morronensis* (VR); *Radiomura cautica* (VR); *Cayeuxia*-type calci-microbes (VR); benthic foraminifera: lituolids (*Gandryina* sp., *Nezzazatinella* sp., *Nautiloculina* cf. *brönnimanni*), loftusiids (cyclamminids, *Charentia* sp., *Vercorsella*/*Montsalevia* sp.), nodosariids (*Bullopora* sp., *Lenticulina* sp.) and miliolids (*Danubiella* sp., *Meandrospira favrei, Troglotella incrustans*) (R-C); agglutinated (R); encrusting benthic foraminifera ?*Coscinophragma* (R); decapod crustaceans *Carpathocancer* (VR)	Planar beds 0.5-2 m thick	Variable texture: packstone with micrite matrix but locally grainstone with rare 10s µm thick rims of isopachous fibrous cement surrounding grains followed by blocky to drusy sparite. Most skeletal grains are micritized (rudists, stromatoporoids, corals) and display borings. The process of micritization is partially evident through destructive-constructive micrite envelopes. Few pressure solution stylolites are locally present filled with ferroan calcite spar. Numerous, multiple generations, fissures filled by blocky calcite or microsparite mosaics	Low-energy, open marine subtidal
F2 – Peloidal and micrite-coated grains packstone/grainstone with crinoids	P/G	Moderately sorted; 0.1-1.5 mm	Peloids (0.1-0.2 mm) (C); micrite coated grains (0.5-1.5 mm) (C); type 4 *Lithocodium*-dominated oncoids (5-6 mm) (S); skeletal grains with thin destructive-constructive micrite envelopes (~0.2 mm) (C)	Crinoids (S); echinoid spines (R); corals (S); *Bacinella-Lithocodium* encrusting corals (S); *Crescentiella morronensis* (VR); benthic foraminifera: nodosariids (*Lenticulina* sp.) and small textulariids (R); dasycladalean algae (VR)	Planar beds 0.5-1 m thick	Micrite matrix fills interparticle space and locally isopachous equant sparite around the grains and blocky sparite. Syntaxial calcite cement sparsely on crinoid ossicles. Skeletal grains are strongly micritized, except crinoids that have thin or no micritic coatings. Sparse sutured grain contacts and stylolites	Low-energy, open to restricted marine subtidal
F3 – Peloidal-crinoidal packstone	P	Well sorted; 0.1-0.7 mm	Peloids (0.1-0.3 mm) (A); micrite coated grains (~0.2 mm) (R); skeletal grains (0.1-0.7 mm) (VC)	Bivalves (R); crinoid ossicles (debris) (A); calcareous sponge fragments (debris) (R); echinoid spines (S); bryozoans (S); decapod crustaceans *Carpathocancer* (R); benthic foraminifera: as nodosariids (*Lenticulina* sp.) (R-S)	Planar beds 0.2-2 m thick	Micrite matrix filling interparticle space. Grains are strongly micritized. Blocky calcite filling fissures	Low-energy, open to restricted marine subtidal
F4 – Peloidal wackestone/floatstone with rudists	W/F	Well sorted; 0.05-1 mm, rarely 8 mm	Peloids (0.05-0.1 mm) (VC); skeletal grains (0.2-1 mm, rarely 8 mm) (VC)	Rudist fragments (C); crinoid ossicles (C); possible bryozoan debris (S); *Lithocodium* fragments (S); miliolids foraminifera (R); calcispheres (VR)	Planar beds <1 m thick	Micritized skeletal grains. Few fissure generations: 1- filled with microsparite and equant sparite, together with angular clasts of host rock (F4); 2- blocky calcite fissure cutting the 1 generation. Stylolites with iron-oxides postdating the 1 fissure generation	Low-energy, restricted subtidal
F5a – Coral boundstone	B, locally W		Peloids (0.06-0.9 mm) (R); tangential ooids (VR); skeletal grains (S)	Different coral colonies: cerioid and plocoid (A); echinoid spine (VR); monaxon siliceous sponge spicules (R); serpulids (R); benthic foraminifera: small textulariids (VR)	~1.5 m thick beds	Locally fissures, few mm thick, filled with silty yellowish material. Within the corallites wackestone with silt-sized skeletal debris	Low- to moderate-energy subtidal
F5b – Stromatoporoid-clotted peloidal micrite boundstone	B-to-W		Peloids (0.06-0.1 mm) (C)	Rudist shells (C); ostracods (VR); *Lithocodium* (C); *Crescentiella morronensis* (VR); chaetetid-type demosponge (C); stromatoporoids (C); serpulids (S); dasycladalean fragment (VR)	~0.5 m thick beds	Micrite matrix. Locally brecciated with blocky sparite and fine micrite matrix with peloids between the angular clasts (<0.5-1 mm-size). The brecciated part is cut by fissures filled by blocky sparite. Fissures with fine, structureless micrite filling are sparse	Low- to moderate-energy subtidal
F5c* – Bacinella *boundstone	B-to-W		Peloids (0.05-0.3 mm) (C)	Ostracods (VR); *Bacinella* (A); siliceous sponges with monaxon spicules (C); *Lithocodium* (R); *Crescentiella morronensis* (VR); gastropod shells (VR-R); benthic foraminifera (R): miliolids and small textulariids; dasycladalean algae *Suppiluliumaella* sp. (R)	~1.5 m thick beds	Micrite and granular sparite cement reflecting the geopetal filling in ostracods. Voids with equant cement in *Bacinella* boundstone and siliceous sponge. Locally crystal silt sediment fill. Stylolites formed around siliceous sponge bodies	Low- to moderate-energy subtidal
F6 – Peloidal packstone with benthic foraminifera and fenestrae	P, locally G	Well sorted; 0.08-1.5 mm	Peloids (0.08-0.1 mm) (VC); oncoids type 3 (1.5 mm) (S); micrite coated grains (~0.2 mm) (R); radial ooids type 1 (~0.5 mm) (R); skeletal grains (0.1-1.5 mm) (VC)	Benthic foraminifera (VC): small loftisiids (*Dobrogelina* sp.), miliolids, textulariids and lituoiids; bivalves (R); gastropods (S); *Cayeuxia* (S); crinoids (R); undetermined calcareous sponges (S); dasycladalean algae (VR); protohalimedacean algae (*Carpathocodium anae*) (R); *Carpathocancer* (VR)	Planar beds 0.5-1.5 m thick	Isopachous fibrous cement surrounding grains, equant cements filling interparticle space and micrite matrix. Skeletal grains strongly micritized. Fenestrae filled with micrite and granular cement, reflecting geopetal structures	Low-energy, open to restricted marine subtidal
F7a – Monomictic breccia	R, clasts W/P	Poorly sorted; 0.01-20 mm	Angular clasts of F8 (0.5-20 mm) (VC); peloids (0.01-0.1mm) (C); skeletal grains (~0.5 mm) (C)	Bivalves (R); crinoids (VC); bryozoans (R-C); *Lithocodium* (VR); unidentified calcareous sponges (VR); coral fragments (S); dasycladalean algae *Suppiluliumaella* sp. (R-S)	Planar bed up to 1 m thick	Micrite matrix between grains. The space between the breccia clasts is filled by blocky, drusy sparite and fine micrite with peloids	Subaerial exposure, karst dissolution and brecciation
F7b – Monomictic breccia with red iron-oxide matrix	R	Poorly sorted; 0.5->20 mm	Angular clasts (0.5-20 mm) (A)	–	One bed 0.5-1.5 m thick	Red, iron-oxide rich matrix. Stylolites filled by insoluble Fe rich material. Clasts of blocky to granular sparite replacing the original texture	Subaerial exposure, karst dissolution and brecciation
F8 – Peloidal wackestone/floatstone with bryozoans	W/F	Moderately sorted; 0.06-3 mm, rarely >6 mm	Peloids (0.06-0.3 mm) (VC); micrite coated grains (R); *Bacinella*-dominated type 4 oncoids (R); skeletal grains (0.2-3 mm, rarely >6 mm) (A)	Rudists (R); bivalves (S); gastropods (VR-R); ostracods (S); crinoids (C); bryozoans (C); *Bacinella*-dominated type 4 oncoids with miliolids foraminifera *Troglotella incrustans* (R); *Lithocodium* (R); undetermined encrusting calcareous sponge (S); stromatoporoid fragments (R); *Carpathocancer* (VR)	Planar beds <1 m thick	Micritized skeletal grains. Locally stylolites	Low-energy, restricted shallow subtidal
F9 – Packstone to rudstone with micritized grains and pisoids	P to R	Moderately sorted; 0.5-6 mm	Skeletal grains (0.5-1 mm) (C); pisoids and micritized grains (1.2-5 mm) (VC)	Rudist shell fragments (at the nucleus of the micritic nodules) (C); bivalves (R); ostracods (VR); gastropods (R); monaxon siliceous sponge spicules (R); benthic foraminifera: textulariids (VR)	Planar beds 0.5-1 m thick	Intensive micritization of pisoids, or possible of oncoids. Micrite meniscus cement. Few-mm irregular sized voids with granular sparite. Locally sparite filling vugs between the pisoids. Rudist shells partially sparite replaced. Numerous pressure solution stylolites	Low-energy, intertidal-supratidal

Tab. 1 - Descriptions of the carbonate facies and related microfacies from F1 to F17 identified in the studied Lower Cretaceous succession. Abbreviations for the abundance in volume percentage (Flügel 2010): VR (very rare; < 2% grains), R (rare; 2–5%), S (sparse; 5–10%), C (common; 10– 30%), VC (very common; 30–50%), A (abundant; > 50%). Texture types (Dunham 1962; Embry & Klovan 1971): W (wackestone), P (packstone), G (grainstone), R (rudstone), B (boundstone).

Facies	Texture	Sorting and grain size	Grain types	Skeletal grains	Bedding	Diagenetic features	Depositional environment
F10 – Siliceous sponge spicule wackestone to packstone with pisoids and fenestrae	W to P, B	Well to moderately sorted; 0.5-3.5 mm	Pisoids and micritized grains (1.5-3.5 mm) (C); skeletal grains (0.5-1.5 mm, rare 3 mm) (VC)	Ostracods (R); monaxon sponge spicules (VC); siliceous sponges, possible demosponges (C); benthic foraminifera: loftusiids, miliolids and textulariids (S)	Planar beds 0.5-1 m thick	Irregular sized fenestrae and vugs within siliceous sponge bodies, filled by laminated crystal silt and equant sparite forming geopetal fillings. Strongly micritized grains. Numerous stylolites postdating sparite filling fissures, fenestrae and dissolution vugs	Low-energy, intertidal-supratidal
F11a – Peloidal-skeletal packstone with* Bacinella *boundstone	P, locally G, B	Well sorted; 0.05-0.3 mm	Peloids (0.05-0.1 mm) (VC); micrite coated grains (~0.2 mm) (S); skeletal grains (0.1-0.3 mm) (VC); *Bacinella*-dominated type 4 oncoids (1-4 mm) (R)	Bivalves (C); gastropods (R); *Cayeuxia* (S); benthic foraminifera: lituolids (*Haplophragmoides* sp.), loftusiids (*Scythiolina* sp., pfenderinids), miliolids and textulariids (VC)	Planar beds 0.5-1.5 m thick	Micrite matrix and intraparticle space filled by isopachous cement around the edge and equant sparite filling. Skeletal grains strongly micritized. Bio-molds of gastropods filled by blocky sparite	Low-energy, intertidal-supratidal
F11b – Peloidal-skeletal packstone to grainstone	P to G	Well sorted; 0.08-1.5 mm	Peloids (0.05-0.1 mm) (C); skeletal grains (0.1-1.5 mm) (VC)	Benthic foraminifera: loftusiids (*Scythiolina* sp., *Siphovalvulina* sp.), miliolids and textulariids (VC); bivalve fragments (VR); gastropods (VR)	Planar beds 0.5-1.5 m thick	Interparticle space filled by isopachous fibrous cement, equant sparite and micrite matrix. Locally meniscus cement binding grains. Skeletal grains strongly micritized. Voids filled by micrite and granular sparite cement	Low-energy, shallow subtidal to intertidal-supratidal
F12 – Peloidal-oncoidal packstone to grainstone with fenestrae	P to G	Moderately sorted; 0.05-7 mm	Peloids (0.05-0.25 mm (VC); skeletal grains (0.2-2 mm) (C); *Bacinella*-dominated type 4 oncoids (1-7 mm) (C); micritized tangential ooids (type 1) and elongated tangential ooids (type 2) (S)	Rudist shells (at nucleus of the oncoids type 4) (R); gastropods (S); benthic foraminifera: involutinids (?*Coscinoconus* sp.), loftusiids (*Scythiolina* sp., *Cribellopsis* sp., *Siphovalvulina* sp.), lituolids (*Haplophragmoides* sp., ?*Bolivinopsis* sp.), miliolids and textulariids (VC); *Cayeuxia* (S)	Planar beds 0.5-1.5 m thick	Few cement types: vadose meniscus microsparite cement at grain contacts; isopachous fibrous sparite around grains and equant cement in the interparticle space, and filling voids. Micrite matrix. All grains are micritized. Fenestrae filled by blocky sparite	Low-energy, intertidal-supratidal
F13 – Peloidal wackestone to packstone with benthic foraminifera	W to P	Well sorted; 0.07-0.4 mm, rarely 4 mm	Peloids (0.07-0.1 mm) (VC); skeletal grains (0.2-0.4 mm, rare 4 mm) (A); calci-mudstone intraclasts (>0.4 mm) (VR)	Benthic foraminifera: lituolids (*Haplophragmoides* sp.), loftusiids (*Scythiolina*/*Vercorsella* sp., *Orbitolinopsis* sp., *Cribellopsis* sp., *Montsalevia salevensis*, ?*Moulladella jourdanensis*), miliolids (*Danubiella gracillima*) and spirilliniids (*Glomospira* sp.) (A); bivalves(R); gastropods (R); *Lithocodium* encrusting bivalve shell (R); *Crescentiella morronensis* (VR); undetermined calcareous sponge (S); *Carpathocancer* (R)	Planar beds 0.5-1 m thick	Micritized skeletal grains	Low-energy, restricted subtidal
F14 – Sponge spicule packstone with chert	P	Well to moderately sorted; 0.06-1 mm	Peloids (0.06-0.1 mm) 10%; skeletal grains (0.1-1 mm) 90%	Bivalves (R); crinoids (R); siliceous sponges (C); possible lithistids (VR); monoaxon siliceous sponge spicules (A); triaxon siliceous sponge spicules (R); crustaceans *Carpathocancer* (R); bryozoans R; benthic foraminifera (R)	0.2-0.5 m thick beds	Silicification with microcrystalline quartz and chalcedony replacing sponge bodies and locally calcitized sponge bodies. Bitumen occurrences in the intergranular space and stylolites	Moderate to high-energy, subtidal to deeper environment
F15 – Peloidal-crinoidal packstone with sparse bryozoans	P, locally G	Well to moderately sorted; 0.1-0.7 mm	Peloids (0.1-0.3 mm) (A); micrite coated grains (~0.2 mm) (S); radial ooids type 1 (~0.5 mm) (VR); (VR); skeletal grains (0.1-0.7 mm) (VC); phosphate grains (VR); quartz grains	Bivalves (R); crinoid ossicles (A); siliceous sponges (R) (above F14); calcareous sponge fragments (debris) (R); echinoid spines (S); bryozoans (S); decapod crustaceans *Carpathocancer* (R); benthic foraminifera: possible loftusiids, miliolids, nodosarids (*Lenticulina* sp.) and textulariids (C)	Planar beds 0.2-2 m thick	Chalcedony replacing siliceous sponge spicules. Grains are strongly micritized and exhibit micro-borings. Micrite matrix or locally blocky calcite cement. Bitumen-bearing sutured grains contacts. Blocky calcite filling fissures	Moderate to high-energy subtidal, possible storm influence
F16 – Red-colour crinoidal packstone with benthic foraminifera, sparse glaucony and quartz grains	P	Well to moderately sorted; 0.1-1 mm, locally 1.5 mm	Peloids (~0.1 mm) (C); skeletal grains (0.3-1.5 mm) (A); glaucony pellets (S); phosphate pellets (VR); quartz grains (S)	Crinoid ossicles (A); bryozoans (C); siliceous sponges? (R); crustaceans *Carpathocancer* (C); benthic foraminifera: miliolids (as *Meandrospira favrei*) (S)	Planar beds 0.3-0.5 m thick	Pressure solution with sutured grain contacts and stylolites Fe oxide residual material. Micrite and mixed clay Fe oxide matrix, and locally blocky sparite. Fe and Mn oxide filling endolithic micro-borings; intraparticle pores in bryozoans and some foraminifera; Fe-oxide coatings on different skeletal grains; ferroan calcite replacement of crustacean fragments	Moderate - energy subtidal to deeper environment
F17 - Peloidal packstone/rudstone with cm-sized lithoclasts, glaucony and quartz grains	P/R	Poorly sorted; 0.5-5 mm, rarely >20 mm	Peloids (0.5-1.5 mm) (C); skeletal grains (0.5-2 mm; rarely >20 mm) (VC); quartz grains (0.01-0.1 mm) (C); glaucony pellets (0.1-0.2 mm) (S); phosphate pellets (VR)	Bivalve and gastropod fragments (R); rudist shell fragments (R); crinoid ossicles (VC); echinoid spines (R); bryozoans (S); benthic foraminifera: textulariids (R)	Planar bed 0.5-1 m thickness (?)	Sutured grain contacts. Lithoclasts of crinoidal packstone with bryozoans with micro-borings and zooids filled by Fe oxides. Rudist shells have red micrite filled borings. Some limestone lithoclasts are red stained by Fe oxides and silicified. Glaucony and detrital quartz grains are rare	Deeper water

Tab. 1 - (see pag. 360).

matoporoids and clotted peloidal micrite (F5b) display various microencrusters including *Lithocodium* and unidentified calcareous sponges (Fig. 7C-D). Clotted peloidal micrite fabric linked to microbially-mediated carbonate precipitation (cf. Della Porta et al. 2003a, 2014 and references therein) is sparsely observed in F5b (Fig. 7E). In F5b beds, there are irregular fissures and vugs with intraclasts of brecciated calci-mudstone within the peloidal micrite matrix (Fig. 7F). Facies F6 is a peloidal packstone with benthic foraminifera and fenestrae (Fig. 7G-H) occurring in the lowermost part of unit I in log A.

The transition into the overlying unit II (30 to 45 m-thick) is marked, in log B by beds of F7a monomictic breccias, with angular lithoclasts and intergranular space filled geopetally by micrite matrix at the base and sparite cement at the top (Fig. 8A-B). In log C, the base of unit II consists of a 0.5-1 m thick layer of F7b breccia with limestone lithoclasts, embedded in a red-colour, iron oxide-rich matrix (Fig. 8C-F). The poorly sorted, angular lithoclasts of F7a breccia are composed of F8 peloidal wackestone/floatstone with bryozoans (Fig. 8B). Facies F8 marks the onset of unit II in log A and contains fine-silt sized fossil debris (Fig. 8G), with rare type 4 *Bacinella*-dominated oncoids with *Lithocodium* laminae (Fig. 8H).

Facies F9 packstone to rudstone contain micritized grains and pisoids with dense micrite coatings (Fig. 9A-B), which are up to 5 mm in size and have nuclei made of intraclasts of packstone with peloids, recrystallized rudist and other bivalve

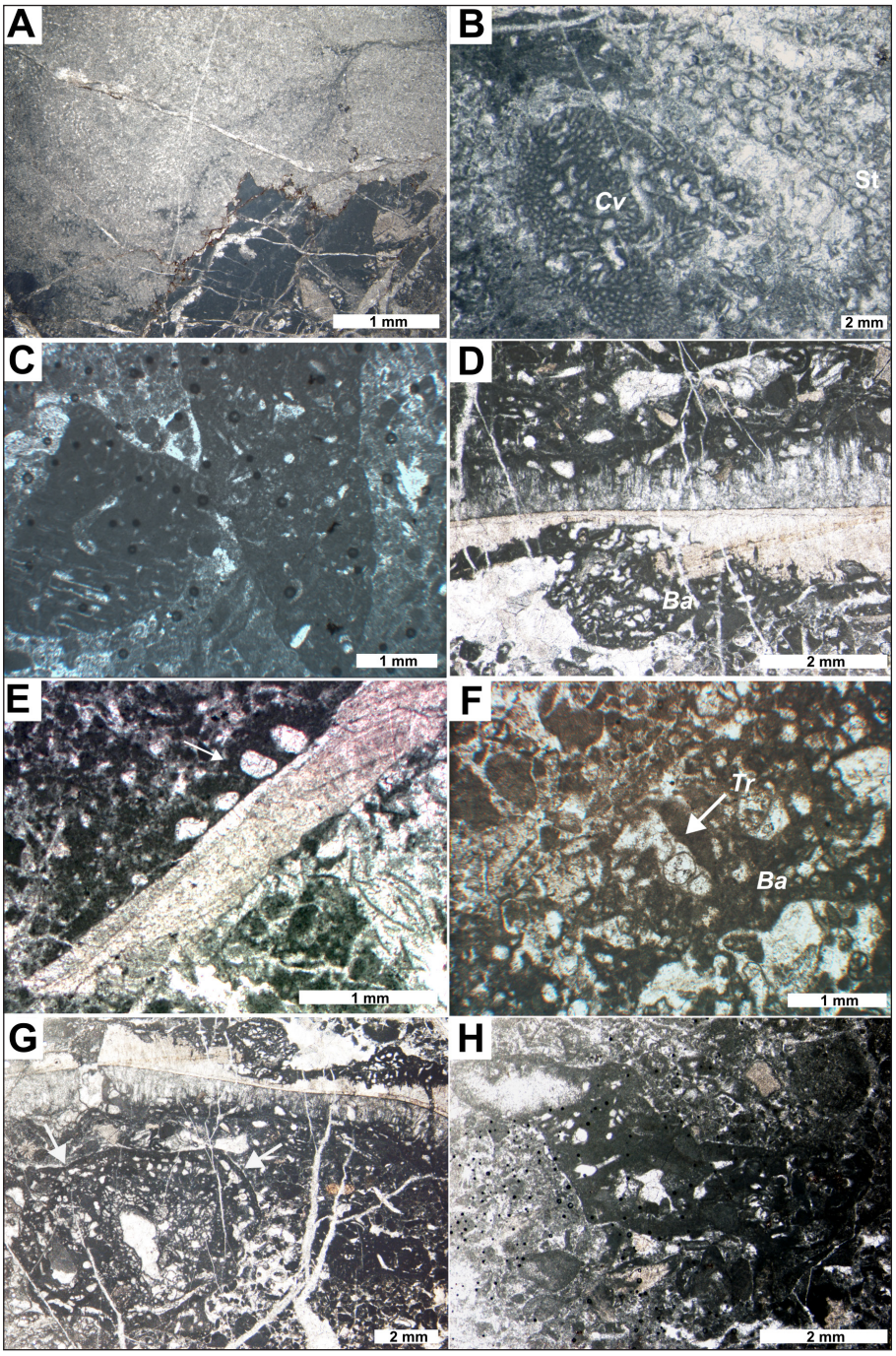

Fig. 5 - Photomicrographs of facies F1 peloidal packstone/grainstone to rudstone with rudists, corals, stromatoporoids and sponges (unit I, logs A and B). A) Possible cerioid coral in F1. Stylolite developed around the coral due to pressure solution (sample A194, log A). B) Calcified sponge *Cylicopsis verticalis* (*Cv*) encrusted by stromatoporoid (St) (sample 305/4, log B). C) Peloidal packstone/grainstone with siliceous sponges (sample A160, log B). D) Rudist shell encrusted by *Bacinella* (*Ba*) (sample 305/7, log B). E) Rudist shell encrusted by foraminifer (white arrow) (sample 303/3, log B). F) Foraminifer *Troglotella incrustans* (*Tr*) perforating *Bacinella* (*Ba*) (sample A0, log B). G) *Bacinella*-dominated type 4 oncoid (white arrow) with few pores filled by micrite and sparite (sample 305/7, log B). H) Irregular *Lithocodium*-dominated type 4 oncoid (sample 305/4, log B).

shells (Fig. 9C). Siliceous sponge spicule wackestone to packstone with pisoids and fenestrae represents facies F10 (Fig. 9D). The irregular dissolution vugs and fenestrae, a few millimetres in size, are geopetally filled by peloidal wackestone at the bottom, sometimes laminated, and equant sparite cement mosaics at the top. Sub-rounded siliceous sponge bodies filled by structureless micrite with numerous vugs are locally marked by stylolites (Fig. 9E) or are embedded in F5c *Bacinella* boundstone (Fig. 9F). The F11a peloidal-skeletal packstone is associated with F5c (Fig. 9G-H) and contains common voids filled by blocky calcite mosaics, in some cases preceded by an isopachous rim of fibrous cement (Fig. 9G-H). F11b peloidal-skeletal packstone to grainstone is well-sorted with common benthic foraminifera and rare sparite-filled voids (Fig. 10A). Facies F12 peloidal-oncoidal packstone to grainstone with fenestrae (Fig. 10B) is characterized by *Bacinella*-dominated type 4 oncoids embedding skeletal grains but lacking distinct nuclei (Fig. 10C) and sparse micritized, tangential type 1 and 2 ooids (Fig. 10D).

In log B, the first level of F7a breccias is overlain by well-sorted F13 peloidal wackestone to

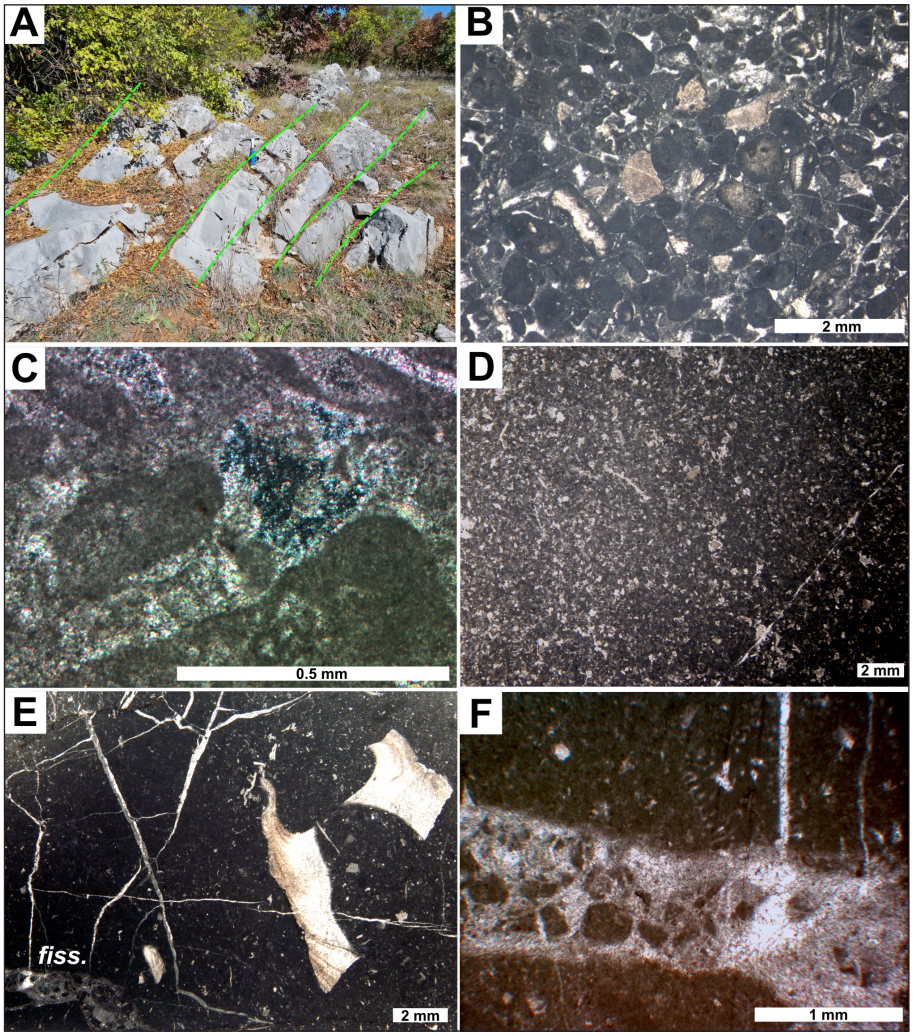

Fig. 6 - Photomicrographs of facies F2, F3 and F4 (unit I, logs A, B and C). A) Outcrop photo of tilted beds of facies F2 and F3 alternating (log C). B) Facies F2 peloidal and micrite-coated grains packstone/grainstone with crinoids (sample D3, log C). C) Isopachous cement of F2 packstone/grainstone with micrite-coated grains (sample 304/1, log B; crossed polarizers). D) Well-sorted peloidal-crinoidal packstone of F3 facies (sample 101/8, log A). E) F4 peloidal wackestone/floatstone with rudists (sample 305/1, log B). F) Fissure in F4 bed (log B) filled by intraclasts of mudstone/wackestone, peloids, microsparite and micrite (sample 305/1, log B).

packstone with benthic foraminifera (Fig. 10E), associated with rare calci-mudstone intraclasts (Fig. 10F). At 190 m in log B, a second level of F7a breccia is characterized by angular clasts of F8 facies with sparse dasycladalean algae. The lower part of unit II in log C comprises F7b breccias with red iron-oxide rich matrix and F8 peloidal wackestone/floatstone capped by a 0.5 m thick dolomite interval. The dolomitized bed is made of nonplanar to planar-s mosaic of replacive anhedral to subhedral dolomite crystals with micritic peloidal nuclei followed by limpid subhedral growth phases (Fig. 10G). Intercrystal porosity is filled by alizarin red-stained, blocky calcite cement (Fig. 10H).

Unit III is marked by a sharp facies change characterized by 0.5 to 4-10 m thick, F14 sponge spicule packstone with chert (Fig. 11A-B). In log A, unit III consists of basal F14, followed by F15 peloidal-crinoidal packstone with sparse bryozoans (Fig. 11C) and siliceous sponge bodies in the lowermost part (Fig. 11D). F16 is a red-colour crinoidal packstone with benthic foraminifera, sparse glaucony and quartz grains (Fig. 11E). Common biota are *Carpathocancer* crustaceans with a distinctive red colour, deriving from iron oxide concentrations (Fig. 11F). In log C, unit III is made of 1.5 m-thick beds of F14, capped by 6 m-thick F15 facies, then followed by poorly sorted F17 peloidal packstone/rudstone with centimetre-sized lithoclasts, glaucony and quartz grains (Fig. 11G-H). Lithoclasts of crinoidal packstone with bryozoans and rare quartz grains are embedded in a peloidal packstone matrix with benthic foraminifera, glaucony and detrital quartz (Fig. 11G-H). Lithoclast contacts are sutured with concentrations of Fe oxides, which also occur within bryozoan intraskeletal space and within tubular micro-borings. The EDX analysis (Appendix 1) confirmed the presence of ferroan oxides (dominantly hematite and magnetite) mostly in the form of dispersed grains in the matrix, and as coating material on skeletal grains. The shells of crustacean *Carpatho-*

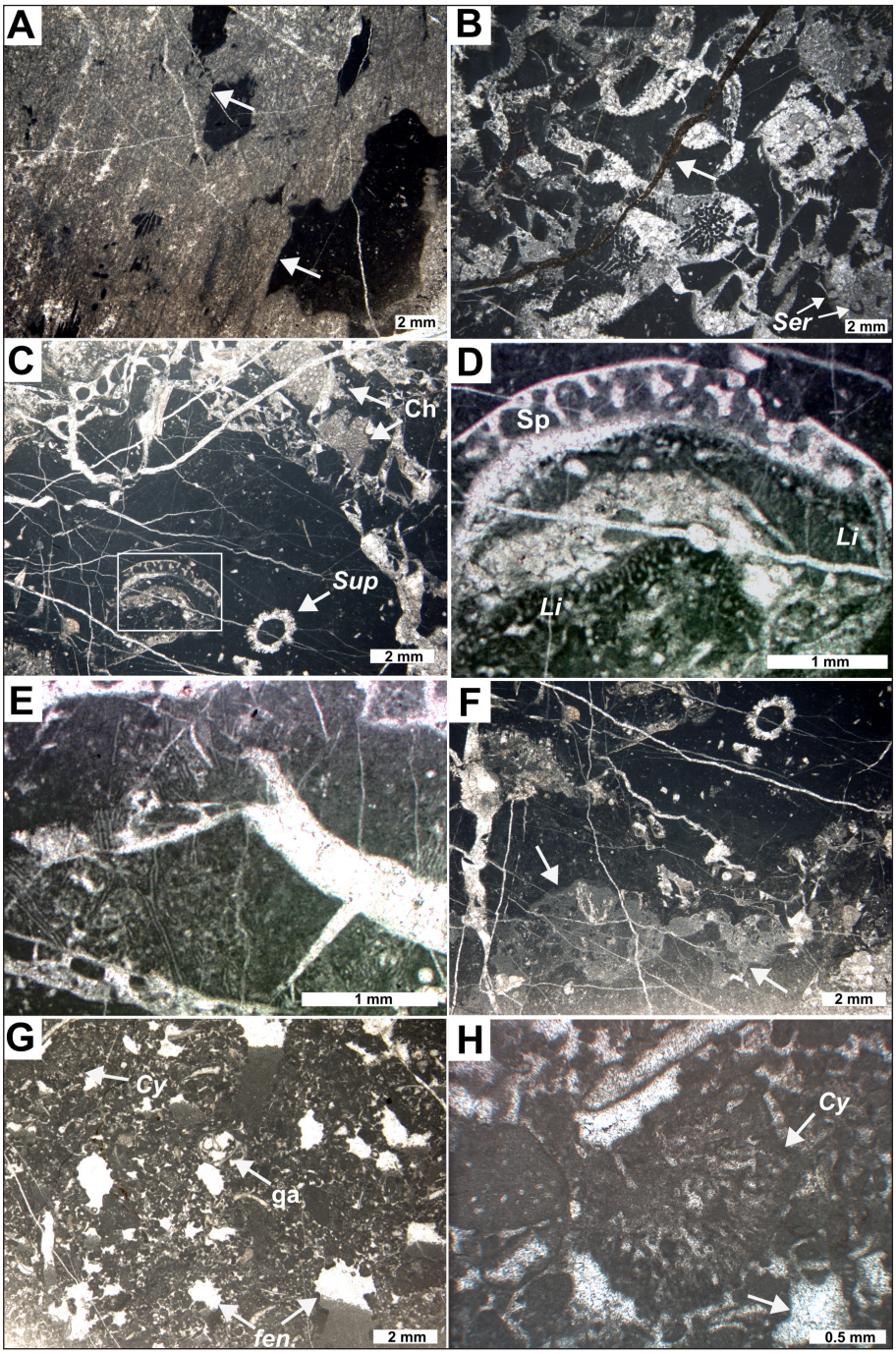

Fig. 7 - Photomicrographs of facies F5a-b and F6 (unit I, logs A and B). A) Facies F5a of cerioid coral colony (white arrows pointing to the corallites) (sample 304/4, log B). B) F5a plocoid coral colony encrusted by serpulids (Ser), locally with skeletal debris wackestone in-between the corallites (sample 101/10, log A). Note the fissure with red-colour siliciclastic sediment with iron oxides and calcite cement (white arrow). C) F5b stromatoporoid-clotted peloidal micrite boundstone, with chaetetid-type demosponge (Ch) (sample 305/8, log B). The white rectangle corresponds to photomicrograph in Figure 7D. Note the algae *Suppiluliumaella* sp. (*Sup*). D) Detail of F5b encrustation framework of *Lithocodium* (*Li*) and unidentified calcareous sponge (Sp) (sample 305/8, log B). E) Detail of clotted peloidal micrite from F5b boundstone showing groups of parallelly arranged thin filamentous structures (sample 305/8, log B). F) Irregular fissures and voids in F5b filled by mudstone angular intraclasts and micrite matrix (white arrows) (sample 305/8, log B). G) Facies F6 peloidal packstone with benthic foraminifera and fenestrae with geopetal filling of micrite and equant sparite (fen.). Sparse to rare skeletal grains in facies F6 are gastropods (ga), bivalves and *Cayeuxia* (*Cy*) (sample 302/2, log A). H) Detail – of F6 showing *Cayeuxia* calci-microbe (*Cy*) and isopachous cement (white arrow) (sample 302/2, log A).

cancer show regular distribution of apatite, calcite and hematite. EDX has identified sparse grains of glaucony, rutile, micas, plagioclase and pyrite. Additionally, in unit III replacive silica is present in the form of small patches (~100 μm wide) in the matrix or on calcite shells.

Biostratigraphic analysis

Benthic foraminifera are scarce within the studied succession. Facies F1 beds from unit I contain rare to sparse benthic foraminifera, especially in the lower part of log B, such as *Charentia* sp. Neumann, 1965 (Fig. 12A-B), *Bullopora* sp. Quenstedt, 1856, *Gandryina* sp. d'Orbigny, 1839, *Nezzazatinella* sp. Darmoian, 1976, *Vercorsella* Arnaud-Vanneau, 1980/*Montsalevia* sp. Zaninetti, Salvini-Bonnard, Charollais & Decrouez, 1987, *Lenticulina* sp. Lamarck, 1804, *Danubiella* sp. Neagu, 1968 (Fig. 12C), *Meandrospira favrei* (Charollais, Brönnimann & Zaninetti 1966) (Fig. 12F-G) and *Nautiloculina* cf. *brönnimanni* Arnaud-Vanneau & Peybernès 1978 (Fig. 12J).

In unit II, facies F13 from log B contains various foraminifera tests: *Scythiolina* Neagu, 2000/*Vercorsella* sp. Arnaud-Vanneau, 1980 (Fig. 12D, E),

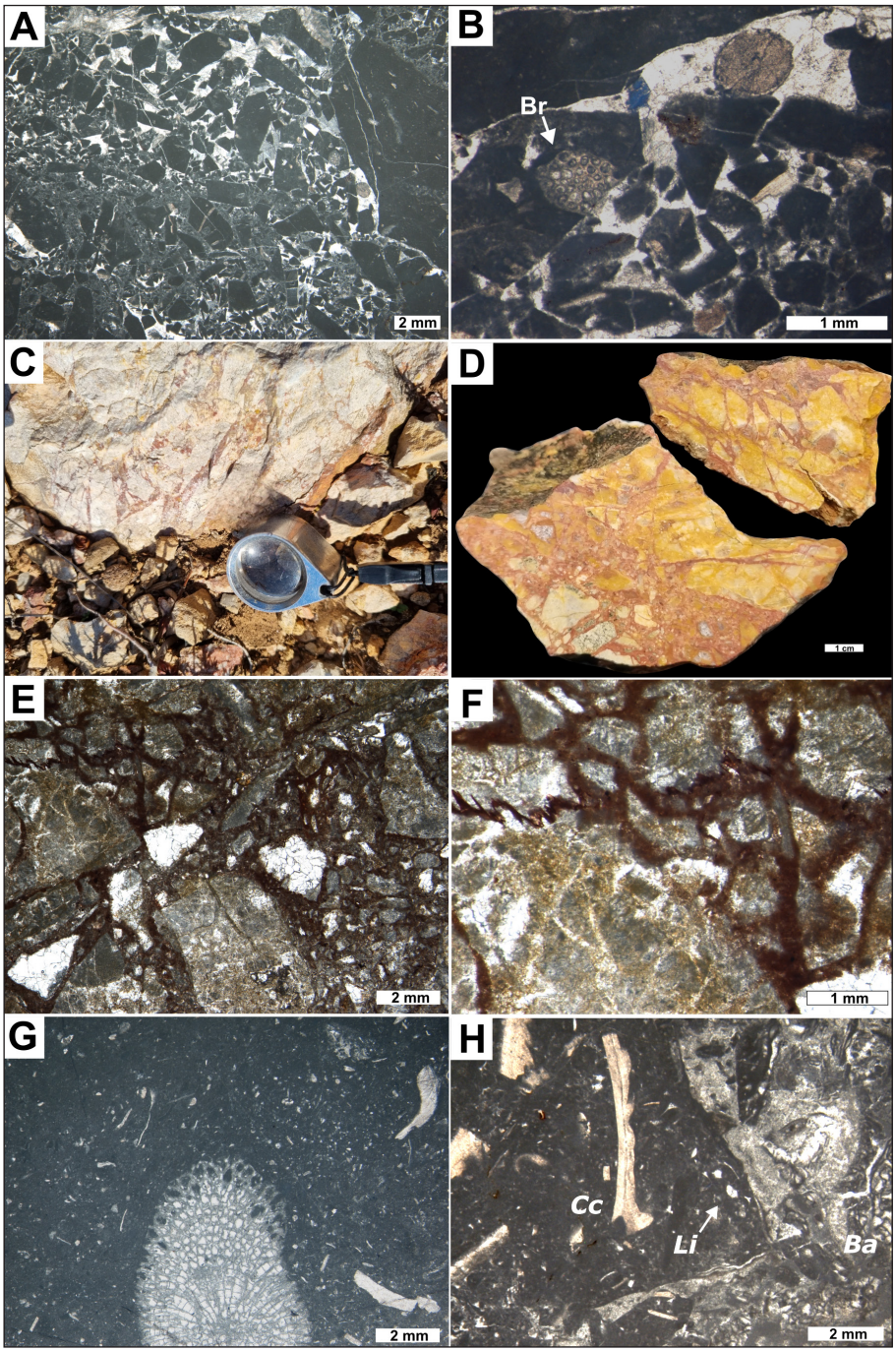

Fig. 8 - Photomicrographs of facies F7a, F7b and F8 (unit II, logs A, B and C). A) Facies F7a of monomictic breccia with angular clasts of F8 peloidal wackestone/floatstone with bryozoans (base of unit II, sample A167, log B). Interparticle space filled geopetally by micrite matrix in the lower part and equant sparite cement in the upper part. B) Detail of crinoid fragment between clasts including bryozoan fragments (Br) in F7a facies (sample A167, log B). C) Outcrop photo of monomictic breccia with red iron-oxide matrix (log C). D) Polished slab of F7b monomictic breccia with red iron-oxide matrix (base of unit II, sample D18.5, log C). E) Photomicrograph of F7b monomictic breccia with red iron-oxide matrix and F) sutured clast contacts in F7b breccias (sample D18.5, log C). G) F8 peloidal wackestone/floatstone with bryozoans (sample D25.5, log C). H) Type 4 *Bacinella*-dominated oncoids (*Ba*) with thin *Lithocodium* crust (*Li*) and *Carpathocancer* fragments (*Cc*) (sample 101/7, log A).

Haplophragmoides sp. Cushman, 1910 (Fig. 12K), *Glomospira* sp. Rzehak, 1885, *Orbitolinopsis* sp. Henson, 1948, and *Cribellopsis* sp. Arnaud-Vanneau, 1980, *Danubiella gracillima* Neagu (Fig. 12L), *Montsalevia salevensis* (Charollais, Brönnimann & Zaninetti) (Fig. 12T) and ?*Moulladella jourdanensis* (Foury & Moullade) (Fig. 12S, U). A similar association is recognized in unit II of log A (facies F11a-b and F12): *Scythiolina* sp., *Haplophragmoides* sp., ?*Coscinoconus* sp. Leupold, 1936 (Fig. 12H), ?*Bolivinopsis* sp. Yakovlev, 1891 (Fig. 12I), *Cribellopsis* sp. (Fig. 12M-P, R), *?Siphovalvulina* sp. Septfontaine, 1988 (Fig. 12Q). In unit III, rare specimens of *Meandrospira favrei* have been identified. The distribution of the identified benthic foraminifera is presented in Figure 13.

In units I and II rare fragments of dasycladalean algae were identified as *Russoella* sp. and *Suppiluliumaella* sp. (Fig. 12V).

Calcareous nannofossil analysis (Elisabetta Erba personal communication) provided barren samples, except one sample from facies F17 peloidal packstone/rudstone with centimetre-sized lithoclasts, glaucony and quartz grains at the top of log C, where the extremely rare nannofossils are re-

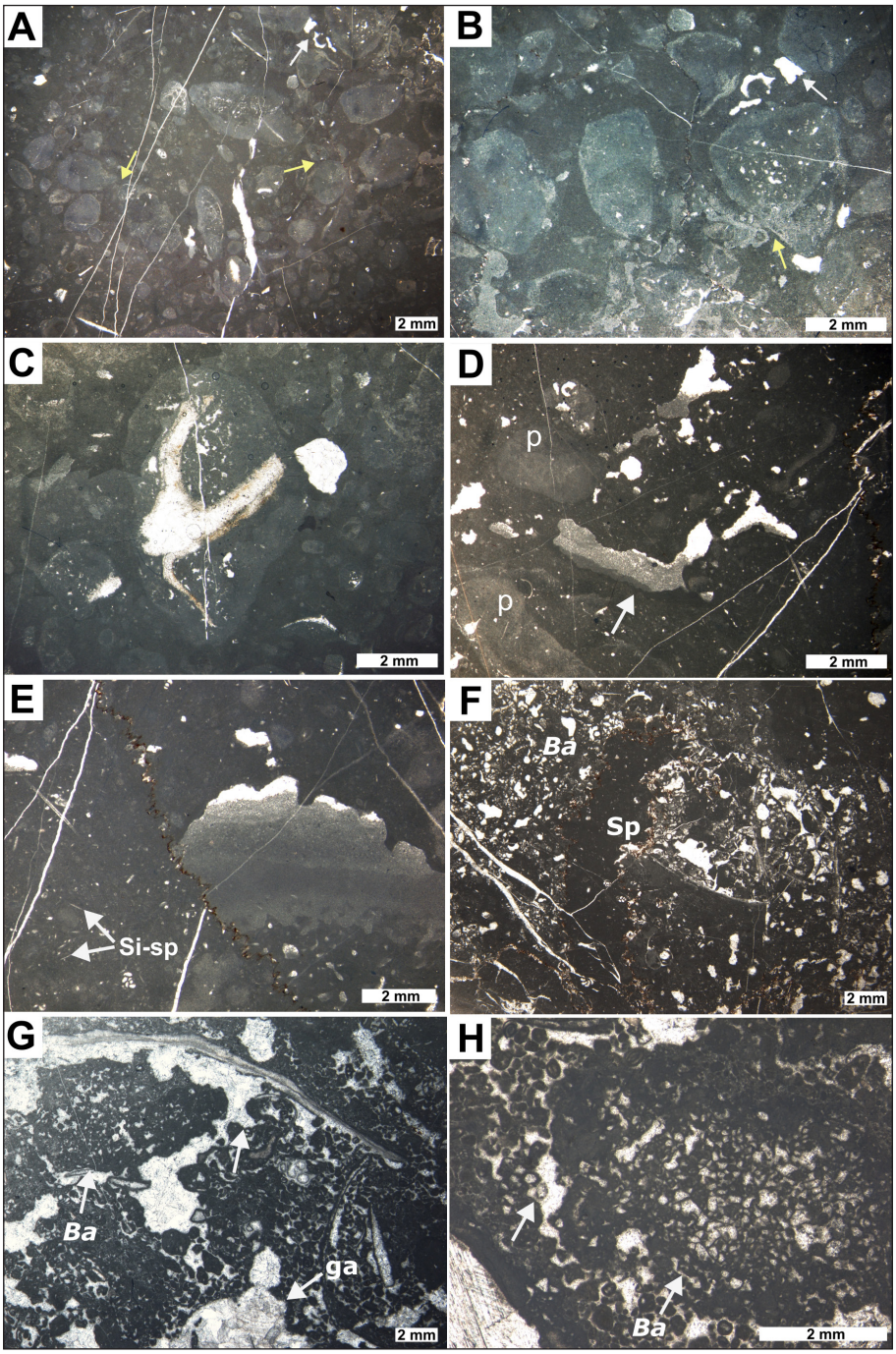

Fig. 9 - Photomicrographs of facies F9, F10, F5c and F11a (unit II, log A). A-B) Photomicrograph of F9 packstone to rudstone with micritized grains and pisoids (sample 101/6, log A). Note the sparite filled voids (white arrows) and small amounts of micritic meniscus cement (yellow arrow). C) Pisoid of F9 with nucleus of peloidal packstone and micritized and recrystallized rudist shell (sample 101/6, log A). D) Photomicrograph of F10 siliceous sponge spicules wackestone to packstone with pisoids (p) and fenestrae-like vugs geopetally filled by vadose crystal silt and equant sparite (white arrow) (sample 101/5, log A). E) Detail of stylolite cutting geopetally filled fenestrae and wackestone to packstone with siliceous sponge spicules (Si-sp) of F10 (sample 101/5, log A). F) Photomicrograph of F5c *Bacinella* boundstone (*Ba*) with siliceous sponge bodies (Sp) in meshwork, partially separated by stylolites (sample 101/4, log A). G) Photomicrograph of F11a peloidal-skeletal packstone with *Bacinella* boundstone (*Ba*). Different skeletal fragments have been recrystallized and replaced by sparite calcite forming a drusy mosaic, as gastropod shells (ga) (sample 101/3, log A). H) Detail of a few millimetres in diameter, *Bacinella*-dominated oncoid type 4 (*Ba*) and isopachous fibrous cement (white arrow).

presented by *Watznaueria barnesiae* (M. Black) Perch-Nielsen 1968 and *Calcicalathina oblongata* (Worsley) Thierstein 1971.

Carbon and oxygen stable isotopes

The results of carbon and oxygen isotope analyses are reported in Table 2 and in vertical trends along the stratigraphic logs (Fig. 13). Figure 14 shows the measured isotopic values plotted per facies of each unit.

In log A, the $\delta^{13}C$ values are fairly uniform ranging between -1.9 and 2.6 ‰ (average 1.6 ‰, standard deviation 0.9), whereas $\delta^{18}O$ varies from -5.9 to -0.8 ‰ (average -2.5 ‰, standard deviation 1.2). In the upper part of unit I (at 35 m in log A), both carbon and oxygen curves show a co-variant decrease of -2 ‰. In unit II, the $\delta^{13}C$ values are uniform, instead the $\delta^{18}O$ first increases up to ~ -1.5 ‰ and then decreases to ~ -3.5 ‰. In unit III, a marked negative excursion for both $\delta^{13}C$ and $\delta^{18}O$ curves is observed at the boundary between facies F15 and F16 (at 100 m in log A).

In log B, the $\delta^{13}C$ values are relatively uniform ranging from 0.6 to 2.1 ‰ (average 1.5 ‰, standard

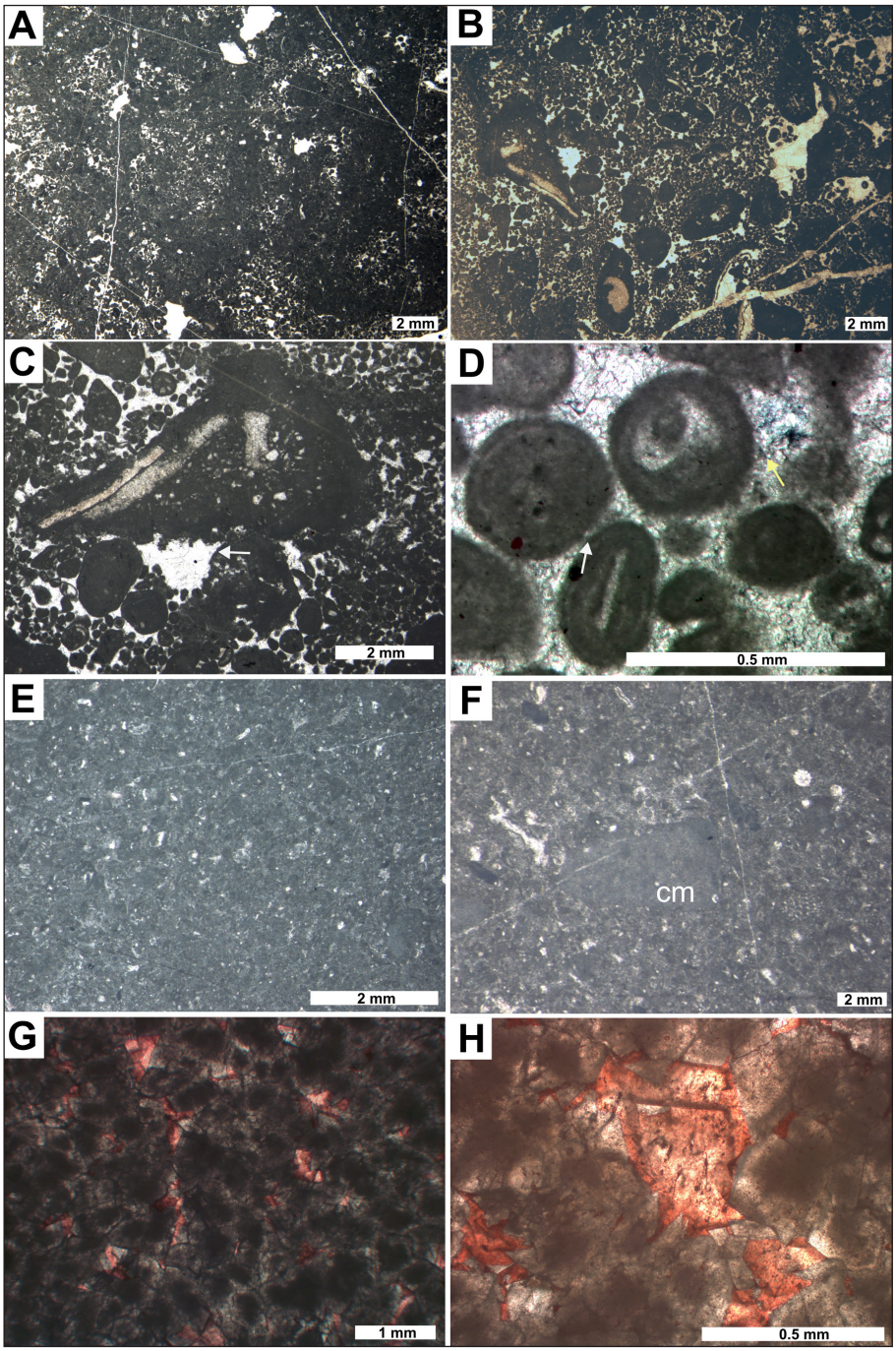

Fig. 10 - Photomicrographs of facies F11b, F12, F13 and dolomite level (unit II, logs A, B and C). A) Photomicrograph of F11b peloidal-skeletal packstone to grainstone. Common skeletal grains are micritized benthic foraminifera (sample 101/1, log A). B) Facies F12 peloidal-oncoidal packstone to grainstone with fenestrae with numerous *Bacinella*-dominated type 4 oncoids embedding few skeletal fragments, but without clearly identified nuclei nor micritic laminae (sample 101/2, log A). C) Detail of *Bacinella*-type oncoid and fenestre filled with blocky sparite (white arrow) (sample 101/2, log A). D) Detail of micritized tangential ooids (type 1) and elongated tangential ooids (type 2), vadose meniscus microsparite cement (white arrow) and isopachous fibrous cement (yellow arrow) of F12 (sample 101/2, log A). E) Facies F13 peloidal wackestone to packstone with benthic foraminifera (sample A177, log B). F) Detail of benthic foraminifer possibly ?*Cribelopsis* sp. of facies F13 and calci-mudstone intraclasts (cm). G) Photomicrograph of dolomite of nonplanar to planar-s (anhedral to subhedral crystals) dolomite with occurrence of intercrystal blocky sparite (pink coloured). Note the micritic nuclei (sample D28.5, log C). H) Detail of pink stained blocky calcite filling the intercrystal pore space in the dolomite mosaic.

Tab. 2 - Minimum, maximum and average values and standard deviation per log, and additionally values for calcite fissures of different facies (CC fractures).

	$\delta^{13}C$				$\delta^{18}O$			
	MIN	MAX	Averages	Standard deviation	MIN	MAX	Averages	Standard deviation
Log A (n=24)	-1.9	2.6	1.6	0.9	-5.9	-0.8	-2.5	1.2
Log B (n=28)	0.6	2.1	1.5	0.6	-4.6	-1.7	-3.1	0.8
Log C (n=16)	-2.1	2.4	1.4	0.6	-9.2	-1.1	-3.5	2.4
CC fractures (n=10)	-2.2	2.2	1.0	1.1	-9.4	0.2	-4.3	3.3

deviation 0.6). The $\delta^{18}O$ values show larger variations ranging from -4.6 and -1.7 ‰ (average -3.1 ‰, standard deviation 0.8). In unit I there are two negative trends around 30 m and 150 m. In unit II, $\delta^{18}O$ gradually decreases to -2.7 ‰, reaching the lowest values at the top of F2 facies, just below the upper F7a breccia level at ~188 m. The lower breccia bed at the base of unit II has $\delta^{13}C$ values of 1.6 ‰ and

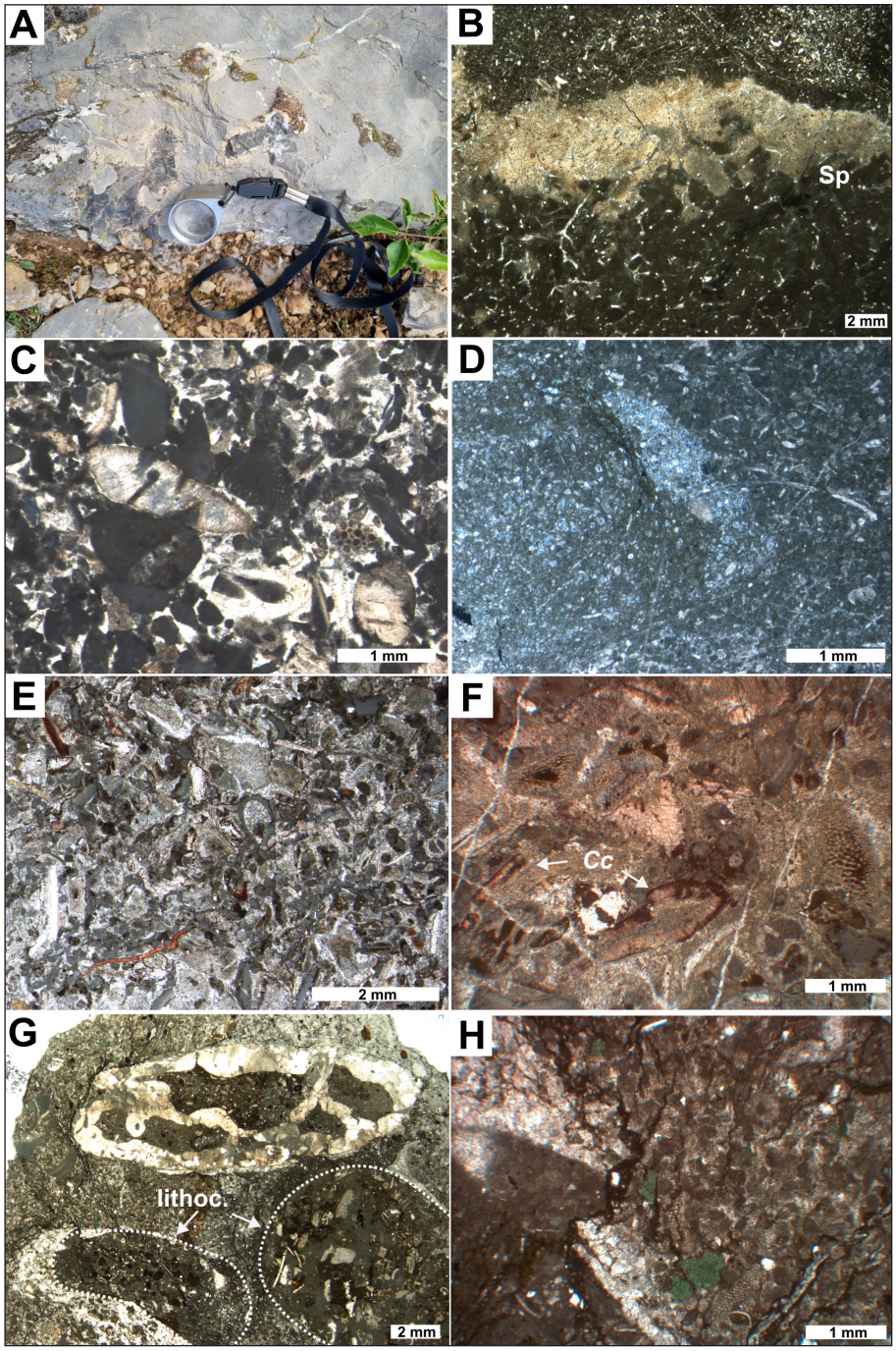

Fig. 11 - Photomicrographs of facies F14, F15, F16 and F17 (unit III, logs A, B and C). A) Outcrop photo of F14 sponge spicule packstone with chert (log B). B) Photomicrograph of F14 with lithistid sponge (Sp), monaxon sponge spicule packstone and silicified patch. Monaxon sponge spicules are concentrated around the sponge body (sample D55, log C). C) Photomicrograph of F15 peloidal-crinoidal packstone with sparse bryozoans (base of unit III, sample D46, log C). D) Detail of facies F15 microquartz and chalcedony-replaced siliceous sponge body, atop of facies F14 (sample B7, log A). E) Photomicrographs of F16 red colour crinoidal packstone with benthic foraminifera, sparse glaucony, quartz grains and syntaxial overgrowth cements (sample B21, log A). F) Detail of F16 with red *Carpathocancer* sp. fragment (*Cc*) associated with crinoid ossicles (sample B22, log A). G) Photomicrograph of F17 peloidal packstone/rudstone with cm-sized lithoclasts (lithoc.), glaucony and quartz grains (sample D70, log C). Lithoclast contacts are sutured due to compaction and pressure solution and some lithoclasts are silicified (sample D70, log C). H) F17 peloidal packstone matrix with glaucony and detrital quartz grains (sample D70, log C).

of -3.0‰ for $\delta^{18}O$ for the lithoclasts, while the blocky sparite cement in the breccia intergranular space provides values of 1.3 ‰ for $\delta^{13}C$ and -6.4 ‰ for $\delta^{18}O$. An increase of approximately 1 ‰ for both $\delta^{13}C$ and $\delta^{18}O$ values marks the transition to unit III.

In log C, the carbon and oxygen isotope measurements show the largest vertical variability with the average values of $\delta^{13}C$ 1.4 ‰ (standard deviation 1.1) and $\delta^{18}O$ -3.5 ‰ (standard deviation 2.4). At the base of unit II in log C, both $\delta^{13}C$ and $\delta^{18}O$ show a shift to negative values of -2.1 ‰ and -7.1 ‰, respectively, coincident with the F7b monomictic breccias. One dolomite sample provides $\delta^{13}C$ values of 2.4 ‰ and of -7.8 ‰ for $\delta^{18}O$. In unit III, both $\delta^{13}C$ and $\delta^{18}O$ values decrease with some oscillations.

Interpretation

Depositional environments

The studied upper Berriasian–lower Valanginian succession of the GCP shows three evolutionary stages: 1) shallow, largely subtidal open marine

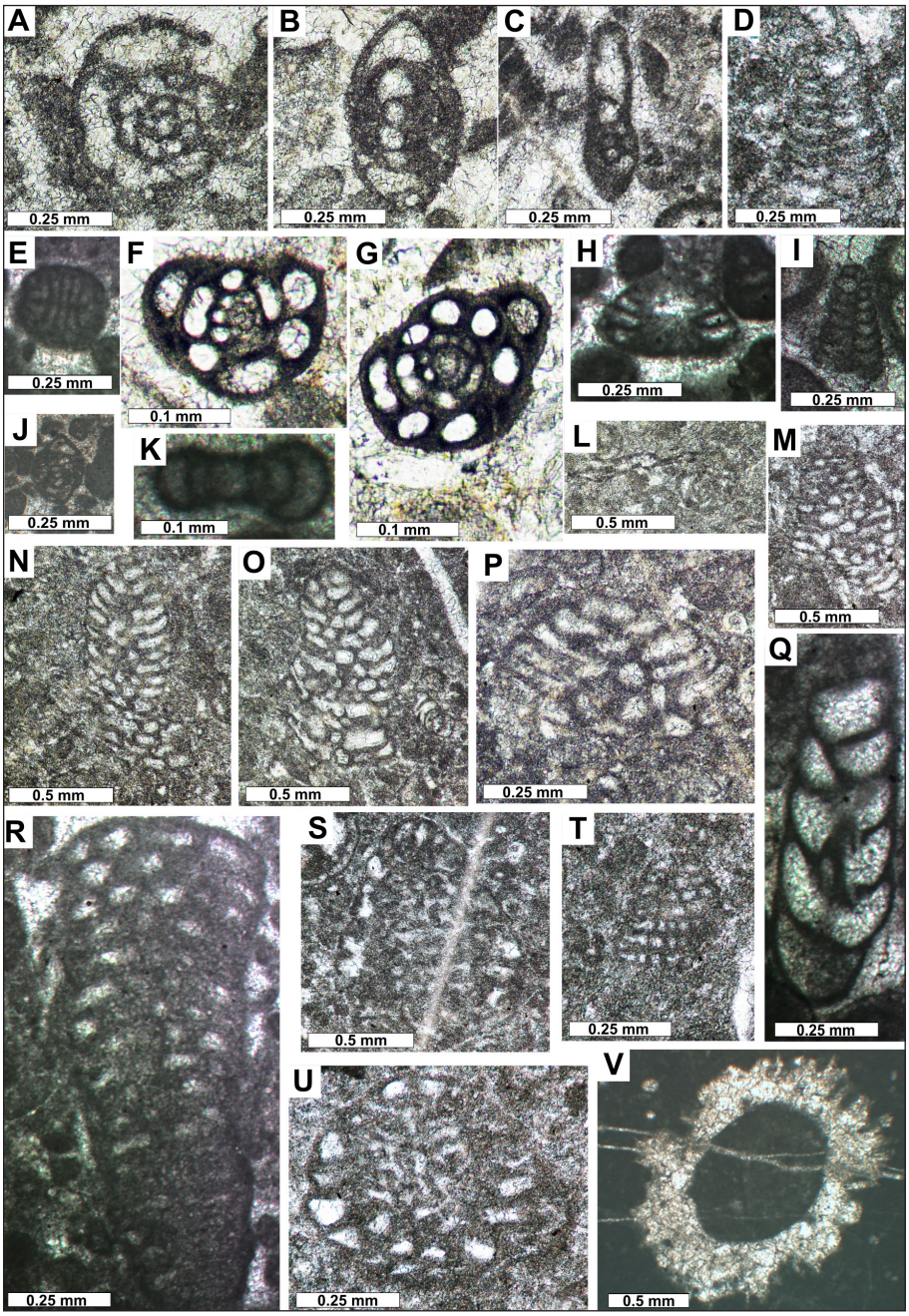

Fig. 12 - Benthic foraminifera and dasycladalean algae of upper Berriasian-lower Valanginian shallow-water carbonates of Dimitrovgrad area. A-B *Charentia* sp. (facies F1; log B; unit I). C *Danubiella* sp. (facies F1; log B; unit I). D-E *Scythiolina* sp. (D – facies F13; log B; unit II; E – facies F11a; log A; unit II). F-G *Meandrospira favrei* (facies F16; log A; unit III). H *?Coscinoconus* sp. (facies F13; log A; unit II). I *Bolivinopsis* sp. (facies F13; log A; unit II). J *Nautiloculina* cf. *brönnimanni* (facies F1; log B; unit I). K *Haplophragmoides* sp. (facies F11a; log A; unit II). L *Danubiella gracillima* (facies F12; log B; unit II). M-P, R *Cribellopsis* sp. (M-P – facies F13; log B; unit II; R – facies F11b; log A; unit II). Q *Siphovalvulina* sp. (facies F11b; log A; unit II). S, U *?Mouladella jourdanensis* (facies F13; log B; unit II). T *Montsalevia salevensis* (facies F13; log B; unit II). V Dasycladalean algae *Suppiluliumaella* sp. (facies F5b; log B; unit I).

sedimentation (unit I), followed by 2) subaerial exposure in some portions of the platform (log B, log C; unit II) and shallowing of the environment of deposition, from subtidal open marine to restricted (log B; unit II) and to intertidal-supratidal setting (log A, log C; unit II), and 3) rapid accommodation creation with deep water siliceous sponges and crinoid-rich red facies indicative of platform drowning (unit III).

Unit I

In unit I, the dominant facies F1 represents deposition in subtidal open marine conditions as testified by rudists, microproblematica *Bacinella* and *Lithocodium*, corals and stromatoporoids. The abundance of micrite matrix and micritized skeletal grains suggests low-energy environments, below the fair-weather wave base (cf. Flügel 2010; Kaya & Altiner 2015; Schlagintweit & Krajewski 2015; Falces-Delgado et al. 2022). *Bacinella* and *Lithocodium* are reported to occur in well-oxygenated waters (Banner et al. 1990; Leinfelder et al. 1993a), in lagoonal to reefal settings forming crusts (Conrad & Clavel 2008), acting as encrusters (Dupraz & Strasser 1999), or forming oncoids in low- to moderate-energy, subtidal lagoons (Dahanayake 1977; Védrine et al.

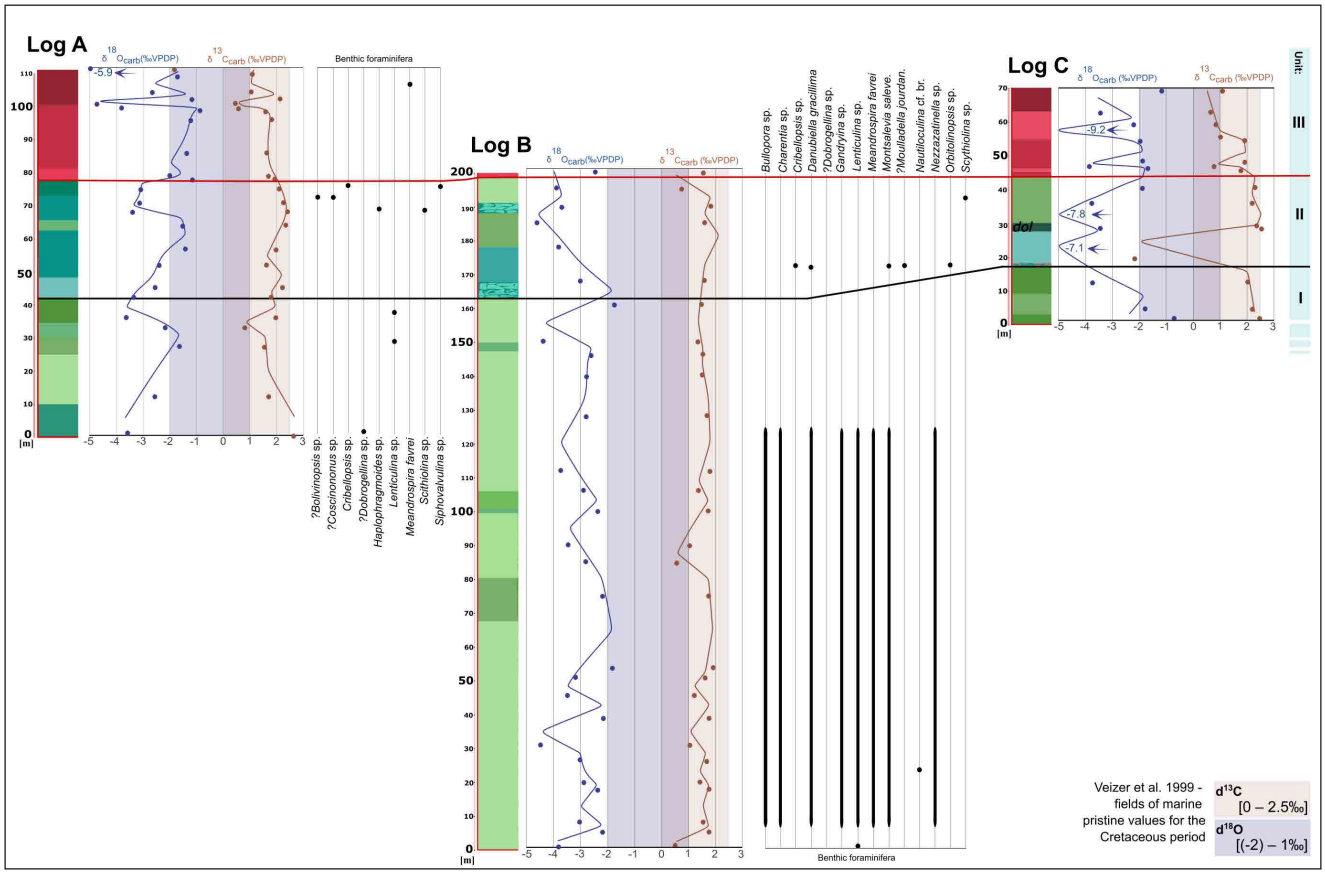

Fig. 13 - Oxygen and carbon stable isotope curves of logs A, B and C and benthic foraminifera distribution (logs A and B). The lowest $\delta^{18}O$ values in logs A and C are indicated by the arrow and the numbers next to it.

2007; Bádenas & Aurell 2010; Sequero et al. 2020). These microproblematica have a corrosive ability (cf. Granier 2021), better developed on the outer wall of dead corals (Bertling & Insalaco 1998), or rudists and benthic foraminifera, as observed in F1 packstone/grainstone facies in this study. Rudists most probably belong to the family of Requieniidae and/or Monopleuridae (Peter W. Skelton personal communication). These rudists dominantly occupied stable sediment or hard substrates in the Early Cretaceous (Ross & Skelton 1993). During the Early Cretaceous, typical reef-builders were corals, siliceous sponges, stromatoporoids and other calcareous sponges (Leinfelder et al. 1996) formed patch reefs with coral-sponge rigid framework surrounded by rudists (cf. Höfling & Scott 2002; Falces-Delgado et al. 2022), as preserved in boundstone facies F5a and F5b. In unit I, the abundance of stromatoporoids might have been favoured by oligotrophic conditions with scarce siliciclastic input, as similarly documented in Upper Jurassic ramps (Leinfelder et al. 2005; Ricci et al. 2018; Nembrini et al. 2021). Facies F2 peloidal and micrite-coated grains packstone/grainstone and F3 peloidal-crinoidal packstone represent the grainy deposits surrounding the F1 decimetre- to metre-scale patch reefs (cf. Nembrini et al. 2021, in Upper Jurassic middle-ramp build-ups in eastern Sardinia, Italy), while F4 wackestone/floatstone corresponds to low-energy subtidal environment.

The irregular fissures filled by red, iron oxide-rich terrigenous sediment (F5a) and those filled by peloidal micrite (F5b) occur approximately at the same stratigraphic level and are interpreted as dissolution features due to meteoric diagenesis. The mineralogical and textural compositions of the fissure-filling material are compatible with terrigenous sediment infill from stratigraphically higher levels during subaerial exposure and meteoric diagenesis (cf. Gonzalez-Donoso et al. 1983; Desrochers & James 1988), at the boundary between unit I and II.

Unit II

The superposition of unit II on unit I is marked by a sharp facies and depositional environment change from open-marine subtidal, below wave-base, and shallow subtidal to supratidal settings, up to

subaerial exposure and erosion. The angular, poorly sorted clasts of F7a breccias, deriving from the erosion of F8 deposits, testify short or no transport. Irregular cracks filled with micrite and red silt are the result of meteoric dissolution and sediment filling in vadose settings followed by blocky sparite as burial cement. This interpretation is supported by the low negative C and O isotope signature of the calcite cements. Beds of the low-energy subtidal facies F8 occur in the lower part of unit II in log A and C and are present as clasts of the F7a breccias in log B and C. F8 was probably deposited across the three logs, but it must have been eroded completely or partly in log B and C. Erosion of subtidal facies, accumulation of breccias with angular clasts showing no transport and the underlying dissolution features filled by iron oxide-rich sediment all agree with a scenario of uplift, subaerial exposure and erosion of marine deposits. The subaerial exposure of subtidal facies may most probably be attributed to syn-sedimentary tectonics where the uplifted footwall fault blocks were affected by subaerial conditions. In other sectors of the study area, shallow water deposition continued in intertidal-supratidal setting (log A) with local early syn-sedimentary replacive dolomitization (log C). In log B, there are two levels of F7a karstic breccias separated by nearly 20 m of subtidal facies (F13, F2) suggesting, at least, two repeated events of subaerial exposure.

Facies (F9, F10) with fenestrae, pisoids, extensive micritization and locally meniscus cement were deposited in intertidal to supratidal environments (cf. Grover & Read 1978; Esteban & Pray 1983; Wright 1994, 2007; Azeredo et al. 2015). In the Permian Capitan Reef platform-top limestones in Texas and New Mexico botryoidal macroids, pisoids with skeletal grains and micrite-rich pisoids were recognized in shallow subtidal to supratidal settings (Esteban & Pray 1983; Della Porta et al. 2004; Verwer et al. 2009). The pisoids with distinct multi-lamellar cortex around nuclei with different fossil fragments are similar to pisoids observed in F9. However, the indistinct to obscure laminae and poorly defined nucleus are typical of micrite-rich pisoids, corresponding to the dominant pisoid type forming F9 facies. These coated grains observed in F9 and F10 could be the result of micritization of biogenic oncoids, as proposed by Esteban & Pray (1983) for the Permian Capitan Reef.

The upper part of unit II consists of marine subtidal (F1, F2, F5a, F11a-b) and intertidal-supratidal facies (F13 only in log A) indicative of renewed accommodation creation. In addition, higher nutrient supply may be inferred from the abundance of siliceous sponges in F5c (cf. Leinfelder et al. 1993b). The abundance of micrite matrix and intense bioclast micritization of F11a and F11b results from deposition in low-energy, subtidal restricted lagoons. The sparse blocky sparite-filled vugs and bio-molds reflect the diagenetic early dissolution and calcite replacement of mollusc aragonite shells (James & Choquette 1984; Tucker & Wright 1990). The abundance of *Bacinella*-type 4 oncoids in F12, associated with common fenestrae, and superficial tangential ooids are indicative of intertidal-supratidal to protected lagoon setting (cf. Grover & Read 1978; Longman 1980; Strasser 1986; Immenhauser et al. 2005). The rare meniscus microsparite cement in facies F11a-b and F12 confirms vadose conditions.

Unit III

A prominent depositional change starts with the sharp deposition of F14 sponge spicules packstone with chert marking the base of unit III. Demosponges, including lithistids, provided siliceous spicules and biogenic silica for the formation of chert observed in F14 (cf. Henrich et al. 1992; Jach 2002; Delecat et al. 2011; Ritterbush 2019). The preserved siliceous sponges and the loose spicules in F14 do not show evidence of being transported by waves or currents (cf. Lackschewitz et al. 1991; Jach 2002). This suggests that facies F14 accumulated in-situ on sea-floors thriving with siliceous sponges as described in other settings (e.g., Delecat et al. 2011; Ritterbush 2019), which later were the main source of silica for the diagenetic chert formation (Hesse 1988, 1989). In marine environments, the concentration of siliceous sponges can be triggered by rapid deepening and substrate availability, water energy, nutrient loading, terrigenous supply and decrease in light availability (Ritterbush 2019). Hence, the sharp superposition of unit III F14 packstone with chert on unit II shallow-subtidal to intertidal-supratidal and exposed facies, represents compelling evidence of transgression, possibly associated with upwelling of nutrient-rich waters, affecting the studied part of the GCP. In fact, a rapid increase in nutrients represents one of the modes to induce the inability of the carbonate system to keep pace with accommodation

creation that further drives the drowning of the carbonate platform (Schlager 1981, 1989).

Unfavourable conditions for shallow, light-dependent photozoan carbonate production, which are conducive to drowning, were probably further enhanced by the increased terrigenous supply (accompanied with an increase in nutrients and turbidity), testified by detrital quartz grains, and other minerals as micas, clay and apatite, in facies F15 and F16. The alternation of facies F14 and F15 in log C is indicative of fluctuations in terrigenous input and environmental energy, probably triggered by marine currents. Hence, the texture and compositional features of facies F14, F15 and F16 in unit III are indicative of a rapid relative sea-level rise creating accommodation and deep, dysphotic to aphotic seafloors associated with nutrient upwelling and siliciclastic input favouring the increase of filter feeders such as crinoids, bryozoans and bivalves, particularly in facies F16. The dominance of these light-independent organisms suggests a mesotrophic environment (Föllmi et al. 1994 and references therein) and a change in carbonate factory from photozoan-dominated carbonate production in unit I and II to heterozoan carbonate association in unit III. The presence of quartz and glaucony grains in facies F15 and F16 confirms the low carbonate sedimentation rates as a consequence of unfavourable conditions for light-dependent oligotrophic carbonate producers (Hallock & Schlager 1986; Föllmi et al. 1994, 2007).

The origin of the red colour of facies F16 crinoidal packstone is due to increased Fe oxide concentrations, as confirmed by the mineralogical composition analyses. Hu et al. (2012) suggested three possible origins for Lower Cretaceous, red colour subtidal marine deposits: 1) detrital origin of oxidized continental iron induced by weathering (e.g., Lajoie & Chagnon 1973); 2) iron-oxidizing bacteria mediation at the time of sedimentation (e.g., Gillan & Ridder 1997; Préat et al. 1999; Boulvain et al. 2001; Della Porta et al. 2003ab, 2004; Kenter et al. 2005; Mamet & Préat 2006; Lazăr et al. 2013); and 3) iron oxidation in highly oxic environments (e.g., Arthur & Fischer 1977). In the investigated samples, numerous red colour micro-structures made of Fe oxides are suggestive of micro-borings and possible microbial influence as described in Mamet & Préat (2006): oxide filling of endolithic tubular irregular micro-perforations; filling of intraparticle porosity within bryozoans and foraminifera chambers; micro-aggregates and coatings around skeletal grains; Fe oxide impregnation of crustacean shell fragments and ferruginous micro-fissures. The supported evidence lies in the resembling bio-textures defined in tens of metres deep, crinoid-rich red limestones identified in Palaeozoic and Mesozoic carbonate settings and interpreted as related to iron oxidizing microbial activity (Boulvain et al. 2001; Della Porta et al. 2003b; Mamet & Préat 2006; Lazăr et al. 2013). Celestino et al. (2017) described red colour, crinoid-rich beds (Upper Jurassic–Lower Cretaceous Rayda Formation, Oman) capping the carbonate platforms affected by extensional tectonics, block-faulting and subsidence (Jenkyns 1991). These red crinoidal limestones were interpreted as the result of episodic storm activity affecting the widespread crinoid meadows thriving in mesotrophic conditions.

Facies F17, identified only in log C, contains clasts of crinoidal packstone with bryozoans with sutured grain contact, embedded in a matrix of peloidal packstone with disseminated glaucony grains indicative of low sedimentation rates (cf. Obasi et al. 2011; Amorosi et al. 2012).

Biostratigraphical age determination

The age determination of the investigated succession relies on benthic foraminifera and calcareous nannofossil associations. There are only few foraminifera-rich strata and an overall lack of reliable biostratigraphic markers; moreover, rare to common benthic foraminifer specimens are often micritized. Nevertheless, the benthic foraminifera association in unit II indicates late Berriasian–early Valanginian age (cf. Bucur & Schlagintweit 2018; Mircescu et al. 2014, 2019). *Montsalevia salevensis* and *Danubiella gracillima* have limited stratigraphic range of Berriasian–early Valanginian (Bucur et al. 1995; Ivanova et al. 2000), while *Moulladella jourdanensis* is commonly reported in the upper Berriasian–lower Valanginian GCP carbonates of Serbia (Bucur et al. 1995, 2020) and Romania (Ungureanu et al. 2015; Grădinaru et al. 2016; Mircescu et al. 2019). Unit III is marked by the rare occurrence of *Meandrospira favrei* that is indicative of Valanginian age (Ivanova et al. 2008). Additionally, Schlagintweit and Bucur (2023) reported the occurrence of orbitolinid *Cribellopsis* sp. in the upper Berria-

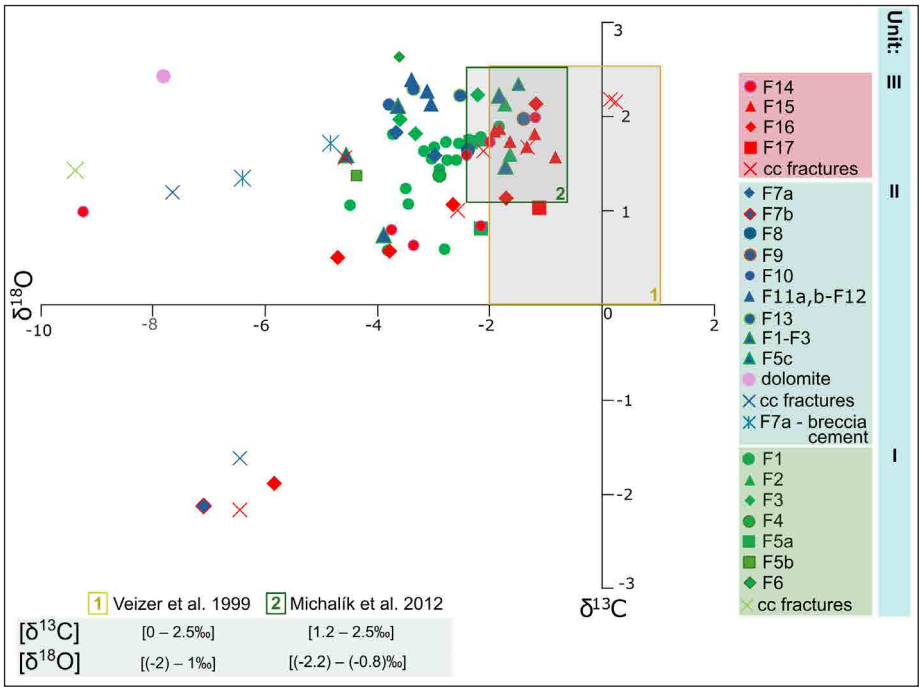

Fig. 14 - Graph showing the distribution of isotopic values by facies in all three units (I-III). The squared values represent fields of stable isotope signatures of $\delta^{13}C$ and $\delta^{18}O$ for Cretaceous period pristine marine carbonates (1 – Veizer et al. 1999) and early Valanginian pelagic limestones from Western Carpathians (2 – Michalík et al. 2012).

sian and upper Valanginian GCP in Romania. The early Valanginian age of unit III has been confirmed by the concomitant occurrence of calcareous nannoplankton *Calcicalathina oblongata* that has a distribution early Valanginian–earliest Barremian (Bown et al. 1998). Hence, the studied section is determined as Berriasian–early Valanginian age.

Interpretation of the carbon and oxygen isotope records

Carbon and oxygen stable isotope measurements provide additional information on the sedimentary evolution of carbonate platforms. The measured C and O stable isotopes (Fig. 14) were compared with $\delta^{13}C$ and $\delta^{18}O$ values expected for the Lower Cretaceous marine pristine carbonates (Veizer et al. 1999) and bulk samples of lower Valanginian pelagic carbonates from the Slovakian Western Carpathians (Michalík et al. 2012). The results from this study only partially fit with the field of Lower Cretaceous pristine marine carbonates (Weissert et al. 1998; Veizer et al. 1999; Weissert & Erba 2004; Michalík et al. 2012).

Log A facies (F2, F9, F15) match the expected values for pristine marine carbonates indicating the lowest meteoric and burial diagenesis resetting. Most of the measured $\delta^{18}O$ values show the influence of burial diagenesis, as demonstrated by the low negative $\delta^{18}O$ values of the cement in the fractures. The burial origin of the F7a cement agrees with the breccia textures with intergranular space filled geopetallly by sediment and cement suggesting that these pores were probably open until burial cement precipitation. The influence of meteoric diagenesis due to subaerial exposure at the base of unit II, as inferred from the F7b breccia textural features, is confirmed by the variable negative $\delta^{18}O$ and $\delta^{13}C$ values indicative of freshwater influence in conditions of high rock/fluid ratio interactions (cf. Allan & Matthews 1982; James & Choquette 1984; Lohman 1988; Morales et al. 2013). The upper part of unit III, dominated by heterozoan carbonate deposits, records low negative isotope values confirming the trend observed by Föllmi et al. (2006) for the Helvetic platform carbonates, where a decrease in isotope values has been interpreted as reflecting the change from photozoan to heterozoan carbonate production.

Discussion

Comparisons across the northern peri-Tethyan Realm

The investigated lowermost Cretaceous sedimentary succession of the Dimitrovgrad area recorded an evolution of the shallow-water platform that resembles other parts of the GCP, such as the Dragoman Block (Ivanova et al. 2008) and Southern Carpathians (Lazăr et al. 2013; Grădinaru et

al. 2016; Pleş et al. 2019). This study documents similar fossil associations, carbonate production modes, and evolution for time-equivalent platforms of the northern Tethyan margin: Jura platform (Föllmi & Godet 2013; Morales et al. 2016), Vocontian Basin (Morales et al. 2013), Helvetic platform (Föllmi et al. 1994; Morales et al. 2016) as well as the intra-Tethyan domain Circum-Rhodope platform (Chatalov et al. 2015).

Units I and II of the investigated GCP in SE Serbia correspond to the shallow-water carbonate sequence of the Slivnitsa Fm., and unit III to the carbonate-terrigenous and terrigenous Salash Fm., of the Bulgarian sector of GCP. In this study, patch reef build-ups have been recognized as in the Slivnitsa Fm., which contains coral-microbial and diceratid-*Bacinella* boundstones, without the formation of large reef complexes (Ivanova et al. 2008; Roniewicz 2008). In the Bulgarian GCP, Ivanova & Chatalov (2022) described a stratigraphic level equivalent to the karstic breccias and subaerial exposure features described in unit II. The Salash Fm. marks the onset of a change from photozoan to heterozoan associations and platform demise (Ivanova & Chatalov 2022), as unit III in the studied Dimitrovgrad succession.

The similarities between the studied southern GCP in SE Serbia and the GCP in Romania concern the peritidal carbonate facies and subaerial exposure features (unit II), overlain by platform drowning (unit III), particularly in the easternmost GCP – Piatra Craiului Dâmbovicioara zone (Barbu & Melinte-Dobrinescu 2008; Grădinaru et al. 2016). Conversely, there are differences in the development of dominant skeletal build-ups (unit I). In Romania reefs are mostly represented by the "Plassen-Štamberk build-ups" cement-rich microencruster-microbialite-calcified sponge hybrid framework (Pleş et al. 2024), while the recognized patch reefs in the investigated area of Dimitrovgrad belong to decimetre-metre scale bioherms of coral-sponge-microencruster type build-ups. In the Romanian GCP, Ungureanu et al. (2015) and Grădinaru et al. (2016) ascribed red colour facies as F15 and F16 in unit III to hemipelagic deposition on distal shelf to slope.

The SE Serbian GCP studied succession shares similarities with the northern Tethys Helvetic platform. The middle Berriasian–lower Valanginian Helvetic platform, cropping out in southern France and Switzerland, consists of the shallow-water Oehrli Limestone (Föllmi et al. 1994, 2007). The Oehrli Limestone was characterized by photozoan carbonate production with bioherms of corals, stromatoporoids and bryozoans switching to the heterozoan carbonates of the Betlis Fm., close to the Berriasian–Valanginian boundary (Föllmi et al. 2007). The boundary between the Oehrli and Betlis lithostratigraphic units is marked by a karstified horizon associated with an iron oxide-stained emersion surface overlain by hardgrounds. Morales et al. (2013) interpreted facies similar to F15 with abundant echinoderm debris, peloids and glaucony grains as deposited in outer shelf settings, influenced by high-energy currents redistributing crinoidal skeletal debris. In fact, the Jura platform of eastern France and western Switzerland (Morales et al. 2013) displays similar evolutionary stages and time frame with the studied Dimitrovgrad succession. The deepening trend on the Jura platform is marked by deposition of the Guiers Member, indicative of an outer shelf environment with benthic foraminifera, echinoderms, bryozoans and *Bacinella*, covered by the upper Member of the Chambotte Formation. This younger unit, rich in benthic foraminifera and rudists, is capped by a palaeosol horizon (cf. unit II) followed by the Bourget Formation with heterozoan carbonates and chert (cf. unit III).

Controlling factors of carbonate platform deposition in northern peri-Tethys during the earliest Cretaceous

The upper Berriasian–Valanginian sedimentary record witnessed significant environmental changes (Föllmi et al. 1994; Weissert & Erba 2004; Föllmi et al. 2012; Föllmi & Godet 2013; Morales et al. 2013, 2016). These changes were expressed through platform drowning episodes and were linked to climate variations, perturbation of the carbon cycles between atmosphere, oceans and biosphere (recorded in the stable isotopes of marine carbonates), changes in hydrological cycle and superficial weathering rates and, consequently, changes in nutrient supply to the oceans and marine carbonate production (Föllmi et al. 2012). The main driving mechanisms of these environmental and sedimentary changes are considered the volcanic activity and CO_2 emissions in the atmosphere coupled with regional tectonic activity (Föllmi et al. 1994; Morales et al. 2013).

Tectonics

The drowning of carbonate platforms may commonly be preceded by subaerial exposure, switching off carbonate production and causing meteoric diagenesis and karst dissolution, especially in tectonically active fault-blocks as evidenced in different Mesozoic carbonate systems (cf. Schlager 1999b; Gawlick & Schlagintweit 2006; Masse et al. 2009; Merino-Tomé et al. 2012). The same scenario is recognized in the studied Dimitrovgrad outcrops, where extensional tectonics along normal faults affected the shallow water carbonate platform (unit I and II) covered by the deeper water facies (unit III).

During the Late Jurassic–Early Cretaceous in the Tethyan Domain (Stampfli and Borel 2002; Stampfli and Horchard 2009), the Dacia Mega-Unit, which constituted the substrate bedrock of the GCP, was located between the Vardar Ocean to the West and the Ceahlau-Severin Ocean to the East (present day positions; Schmid et al. 2008, 2020). Different contractional tectonic phases in the Cretaceous period were reported by van Hinsbergen et al. (2020), with one in particular in the Early Cretaceous starting in the mid-Valanginian (~135 Ma) and lasting until the Cenomanian (~95 Ma), indicating the lack of regional extensional phases during this period. The main phase of formation of the Carpathian orogen was set during the Aptian–Albian time, overprinting the possible extensional effects of the earliest Cretaceous. This possible earliest Cretaceous extensional phase could be related to the activity in the Ceahlau-Severin Ocean domain affecting its western border (e.g. eastern part of GCP). However, the timing and duration of extensional tectonics along the Ceahlau-Severin Ocean lack detailed studies.

Facies similar to those unit III from this study, in the eastern portion of the Romanian GCP, were interpreted by Grădinaru et al. (2016) in the context of sea-level oscillations, extensional tectonics and erosion and collapse of the platform strata due to normal fault activity during the early Valanginian Neo-Cimmerian phase. The effects of the Neo-Cimmerian phase were as well reported in the northern Tethyan platforms (cf. Föllmi et al. 1994; Morales et al. 2013).

The effects of the supposed earliest Cretaceous syn-sedimentary extensional tectonic are recognized in the GCP, but within a poorly defined tectonic regime. The structural geology features of the Dimitrovgrad succession are difficult to be identified in the field due to post-sedimentary orogenetic deformation. However, the depositional facies and the recognized platform evolution through three superimposed units record the influence of active tectonics, as observed in other portions of the GCP, even though the structural evidence is poorly preserved in the studied area.

Nutrients

Föllmi et al. (2012) discussed the sedimentary trends of exported kaolinite, phosphorous-burial and strontium-isotope records reflecting increased nutrient supply and fluxes during the Early Cretaceous. The initial cause of nutrient increase in marine settings was the climate change during late Berriasian–early Valanginian when warmer and more humid conditions led to an increase in weathering rates (Duchamp-Alphonse et al. 2011) and further to enhanced upwelling in the ocean. An increase in nutrients is inferred in the Dimitrovgrad succession because of the abundance of siliceous sponges (F14), as similarly interpreted in the Lower Jurassic of the Northern Calcareous Alps, Austria (Delecat & Reitner 2005). Nutrient increases affect carbonate production leading the change from photozoan to heterozoan biota association (James 1997; Schlager 2000), as seen in unit III. This switch from photozoan to heterozoan association (coral-oolite to crinoid-bryozoan mode sensu Föllmi et al. 1994) was recognized for the early–late Valanginian time in the Tethyan Region (Walter 1989; Frakes et al. 1992) and is directly related to climate warming and increased weathering.

The upwelling of deeper water and sea-bottom sediments over shallow-water carbonate platforms is accompanied by increase in suspended nutrients and particulate organic matter, as reported in recent coastal zone of central California (Mullins et al. 1985). The ocean fertilization during the early-late Valanginian is considered the result of upwelling of colder, nutrient-rich waters from the deeper parts of the basin, following marine transgression (Föllmi et al. 1994; Barbu & Melinte-Dobrinescu 2008; Barbu 2013; Morales et al. 2013, 2016). Additionally, a Valanginian transgressive event was recognized in the Serbian sector of the GCP (Bucur et al. 2020). These authors identified an unconformity, followed by a major transgression corresponding to the Kva1 event in the Cretaceous sea-level curve by Haq (2014).

Conclusions

The lowermost Cretaceous GCP carbonate succession in the Dimitrovgrad area of SE Serbia has been investigated in detail for the first time, integrating sedimentological, biostratigraphical and chemostratigraphical characterization of the carbonate facies through the analysis of three logs A, B and C. The three distinguished sedimentary units (unit I, II and III) reflect three evolutionary stages of the GCP during the Berriasian–early Valanginian.

Unit I consists of rudist-coral-calcareous and siliceous sponges patch reefs with *Bacinella-Lithocodium*, and grainy moderately- to well-sorted packstone to grainstone facies in between boundstone lenses. The 160 metres thick unit I is indicative of deposition in open to marine, well oxygenated, subtidal settings.

Unit II is characterized by different levels of breccia, followed by development of wackestone facies with bryozoans and benthic foraminifera, oncoid- and pisoid-rich facies with fenestrae, and a syn-sedimentary dolomitized bed. Unit II represents a shallowing of the depositional environment with respect to unit I with transition from subtidal open marine facies (unit I) to restrictive subtidal and intertidal-supratidal facies (unit II), postdating the subaerially exposures of the platform top demonstrated by karst collapse breccias. The influence of meteoric diagenesis is confirmed by the negative values of stable oxygen and carbon isotope measured in the karst level breccia. The uppermost part of unit II indicates the re-establishment of normal marine subtidal conditions.

A sharp facies change with siliceous sponge spicule packstone with chert (unit III) on top of inter- to subtidal open marine facies (unit II) marks the boundary between unit II and III. Unit III is rich in crinoids and bryozoans and shows the occurrence of quartz and glaucony grains, and red colour, iron oxide rich matrix. The carbonate-producing biota association changes from photozoan in unit I and II, to filter feeding, heterozoan in unit III, most probably driven by transgression, terrigenous sediment supply and inferred increased in nutrients. The change in carbonate factory, facies types with glaucony and quartz grains, the presence of red iron oxide rich micrite and the low sedimentation rates in unit III are indicative of platform drowning.

The studied Dimitrovgrad upper Berriasian–lower Valanginian carbonate strata with superimposed unit I – normal setting; unit II – subaerial exposure and reestablishment of shallow-water deposition of the platform; and unit III – platform drowning, resemble coeval carbonate successions recording regionally recognized time-equivalent events in the Tethyan realm. The subaerial exposure is most probably the result of syn-sedimentary tectonics and formation of uplifted tilted blocks, as proposed for the Romanian part of the GCP and other carbonate platforms of the northern peri-Tethyan Realm. Subaerial exposure followed by transgression and late Berriasian–early Valanginian global humid climate led to increased nutrient fluxes and further to the platform drowning as recognized in the Dimitrovgrad area.

Data Availability Statement

The data supporting the results of this research are available upon request. Interested researchers may contact the corresponding Author to obtain access.

Acknowledgments: The authors gratefully thank Elisabetta Erba (University of Milan) for calcareous nannofossil evaluation and Peter W. Skelton (Open University) for determination of rudists. Matteo Pegoraro (University of Milan) and Zorica Uskoković (University of Belgrade) are thanked for thin section preparation. Elena Ferrari (University of Milan) for the stable isotope analyses and Jovana Malbašić (University of Belgrade) for the help with SEM analysis. One anonymous reviewer and Felix Schlagintweit are thanked for the useful comments that helped improving the manuscript.

Funding: JS acknowledges the contribution of the Ministry of Education, Science and Technological Development of the Republic of Serbia (Contract no. 451-03-136/2025-03/200126) and benefited from a grant from the Italian Ministry of Foreign Affairs and International Cooperation (MAECI) for the 2022-2023 academic year.

References

Allan J. R. & Matthews R.K. (1982) - Isotope signatures associated with early meteoric diagenesis. *Sedimentology*, 29: 797-817.

Amorosi A., Guidi R., Mas R. & Falanga E. (2012) Glaucony from the Cretaceous of the Sierra de Guadarrama (Central Spain) and its application in a sequence-stratigraphic context. *International Journal of Earth Sciences*, 1: 415-427.

Anđelković J., Krstić B., Bogdanović P., Jadranin D., Milenković P., Milošaković, R., Urošević D., Dimitrijević M., Dolić D., Rakić M.O., Jovanović Lj., Maslarević Lj., Marković B., Divljan M. & Đorđević M. (1969) - Explanatory booklet for sheet PIROT, K 34-34 and BREZNIK, K 34-46 Basic Geological Map of SFRY, 1:100,000. Federal Geological Survey, Beograd, 69 pp.

Anđelković J., Krstić B., Bogdanović P., Jadranin D., Milošaković R., Milenković P., Fotić V. & Jovanović L. (1975) - Basic Geological Map of SFRY, 1:100,000, Sheet Breznik (K

34-46). Federal Geological Survey, Beograd.

Angelov V., Marinova R., Grozdev V., Antonov M., Sinyovski D., Ivanova D., Petrov I., Metodiev L., Milovanov P., Popov A., Valev V. & Aydanliyski G. (2010) - Geological Map of the Republic of Bulgaria. Scale 1:50 000. Dragoman Map Sheet, Ministry of Environment and Water and Bulgarian National Geological Survey.

Arthur M.A. & Fischer A.G. (1977) - Upper Cretaceous–Paleocene magnetic stratigraphy at Gubbio, Italy. Lithostratigraphy and sedimentology. *Geological Society of America Bulletin*, 88(3): 367-371.

Azeredo A.C., Wright V.P., Mendonça-Filho J., Cabral M.C. & Duarte L.V. (2015) - Deciphering the history of hydrologic and climatic changes on carbonate lowstand surfaces: calcrete and organic-matter/evaporite facies association on a palimpsest Middle Jurassic landscape from Portugal. *Sedimentary Geology*, 323: 66-91.

Bádenas B. & Aurell M. (2010) - Facies models of a shallow-water carbonate ramp based on distribution of non-skeletal grains (Kimmeridgian, Spain). *Facies*, 56, 89-110.

Banner F.T., Finch E.M. & Simmons M.D. (1990) - On *Lithocodium* Elliott (calcareous algae); its paleobiological and stratigraphical significance. *Journal of Micropalaeontology*, London, vol. 9, no. 1: 21-36.

Barbu V. & Melinte-Dobrinescu M.C. (2008) - Latest Jurassic to Earliest Cretaceous paleoenvironmental changes in the Southern Carpathians (Romania): regional record of the Late Valanginian nutrification event. *Cretaceous Research*, 29: 790-802.

Barbu V. (2013) - Valanginian isotopic and palaeoecological signals from the Bucegi Mountains, Southern Carpathians, Romania. *Geological Society London Special Publications,* 382: 5-29.

Bertling M. & Insalaco E. (1998) - Late Jurassic coral/microbial reefs from the northern Paris Basin—facies, palaeoecology and palaeobiogeography. *Palaeogeography, Palaeoclimatology, Palaeoecology*, 139(3-4): 139-175.

Boulvain F., De Ridder C., Mamet B., Préat A. & Gillan D. (2001) - Iron microbial communities in Belgian Frasnians carbonate mounds. *Facies*, 44(1): 47-59.

Bown P.R., Rutledge D.C., Crux J.A. & Gallagher L.T. (1998) - Lower Cretaceous. In: Bown P. R. (Eds) - Calcareous Nannofossil Biostratigraphy: 86-131. British Micropalaeontological Society Publication Series.

Bubík M., Cígler V., Mikuláš R., Rabrenović D., Reháková D., Skupien P., Švábenická L., Svobodová A. & Svobodová M. (2024) - The integrated biostratigraphy and palaeoenvironments across the Jurassic–Cretaceous boundary in the Dedina section (eastern Serbian Carpathians). *Cretaceous Research*, 158: 105817.

Bucur I.I. & Schlagintweit F. (2018) - *Moulladella jourdanensis* (Foury & Moullade, 1966) n. gen., n. comb.: Valanginian-early late Barremian larger benthic foraminifera from the northern Neotethyan margin. *Acta Palaeontologica Romaniae*, 14(2): 45-59.

Bucur I.I., Conrad M.A. & Radoičić R. (1995) - Foraminifers and calcareous algae from Valanginian limestones in the Jerma River Canyon, Eastern Serbia. *Revue de Paléobiologie*, 14(2): 349-377.

Bucur I.I., Jovanović D., Radoičić R., Sudar M. & Mircescu C.V. (2021) - Lower Cretaceous carbonate deposits from the Derezna borehole (Carpatho-Balkanides, eastern Serbia) and remarks on some dasycladalean algae. *Acta Palaeontologica Romaniae*, 17(1): 3-14.

Bucur I.I., Sudar M., Schlagintweit F., Pleș G., Săsăran E., Jovanović D., Polavder S. & Radoičić R. (2020) - Lowermost Cretaceous limestones from the Kučaj zone (Carpatho–Balkanides, Eastern Serbia): new data on their age assignment, *Cretaceous Research*, 116: 104575.

Cavalheiro L., Wagner T., Steinig S., Bottini C., Dummann W., Esegbue O, Gambacorta G., Giraldo-Gómez V., Farnsworth A., Flögel S., Hofmann P., Lunt D.J., Rethemeyer J., Torricelli S. & Erba E. (2021) - Impact of global cooling on Early Cretaceous high p CO_2 world during the Weissert Event. *Nature communications*, 12(1): 5411.

Celestino R., Wohlwend S., Rehakova D. & Weissert H. (2017) - Carbon isotope stratigraphy, biostratigraphy and sedimentology of the Upper Jurassic–Lower Cretaceous Rayda Formation, Central Oman Mountains, *Newsletter on Stratigraphy*, 50(1): 91-109.

Chatalov A., Bonev N. & Ivanova D. (2015) - Depositional characteristics and constraints on the mid-Valanginian demise of a carbonate platform in the intra-Tethyan domain, Circum Rhodope belt, northern Greece. *Cretaceous Research*, 78: 55-115.

Conrad M.A. & Clavel B. (2008) - A *Lithocodium* and *Bacinella* signature of a late Hauterivian, local microbial event: the Urgonian limestone in south-east France. *Geologia Croatica*, 61(2-3): 239-250.

Csontos L. & Vörös A. (2004) - Mesozoic plate tectonic reconstruction of the Carpathian region. *Palaeogeography, Palaeoclimatology, Palaeoecology*, 210: 1-56.

Dickson J.A.D. (1965) - A modified staining technique for carbonates in thin section. *Nature*, 205(4971): 587-587.

Dickson J.A.D. (1966) - Carbonate identification and genesis as revealed by staining. *Journal of Sedimentary Research*, 36(2): 491-505.

Dahanayake K. (1977) - Classification of oncoids from the Upper Jurassic carbonates of the French Jura. *Sedimentary Geology*, 18: 337-353.

Delecat S. & Reitner J. (2005) - Sponge communities from the Lower Liassic of Adnet (Northern Calcareous Alps, Austria). *Facies*, 51: 385-404.

Delecat S., Arp G. & Reitner J. (2011) - Aftermath of the Triassic–Jurassic Boundary Crisis: Spiculite Formation on Drowned Triassic Steinplatte Reef-Slope by Communities of Hexactinellid Sponges (Northern Calcareous Alps, Austria). In: Reitner J., Quéric N.V. & Arp G. (Eds) - Advances in Stromatolite Geobiology, Lecture Notes in Earth Sciences: 355-390. Springer Berlin Heidelberg, Berlin, Heidelberg.

Della Porta G., Kenter J.A.M., Bahamonde J.R., Immenhauser A. & Villa E. (2003a) - Microbial boundstone dominated carbonate slope (Upper Carboniferous, N Spain): microfacies, lithofacies distribution and stratal geometry. *Facies*, 49: 175-208.

Della Porta G., Mamet B. & Préat A. (2003b) - Microbial mediation in the formation of red limestones, Upper Carboniferous, Cantabrian Mountains, Spain. Proceedings of the XVth International Congress on Carboniferous and Permian Stratigraphy. Utrecht, the Netherlands, 10-16 August 2003.

Della Porta G., Kenter J.A. & Bahamonde J. R. (2004) - Depositional facies and stratal geometry of an Upper Carboniferous prograding and aggrading high-relief carbonate platform (Cantabrian Mountains, N Spain). *Sedimentology*, 51(2): 267-295.

Della Porta G., Merino-Tomé O., Kenter J.A., & Verwer K.

(2014) - Lower Jurassic microbial and skeletal carbonate factories and platform geometry (Djebel Bou Dahar, High Atlas, Morocco). In: Verwer K., Playton T.E. & Harris P.M. (Eds) - Deposits, Architecture and Controls of Carbonate Margin, Slope and Basinal Settings. Society of Economic Paleontologists and Mineralogists, Tulsa, Special Publications, 105.

Dercourt J., Gaetani M., Vrielynck B., Barrier E., Biju-Duval B., Bruet M.F., Cadet J.P., Crasquin S. & Săndulescu M. (2000) - Atlas Peri-Tethys, Palaeogeographical Maps. 24 maps and explanatory notes. CCGM/CGMW, Paris, 269 pp.

Desrochers A. & James N.P. (1988) - Early Paleozoic surface and subsurface paleokarst: Middle Ordovician carbonates, Mingan Islands, Quebec. In: James N.P. & Choquette P.W. (Eds) - Paleokarst: 183-210. New York, NY: Springer New York.

Dimitrijević M.D. (1997) - Geology of Yugoslavia. Geological Institute, Belgrade. 187 pp.

Duchamp-Alphonse S., Fiet N., Adatte T. & Maurice P. (2011) - Climate and sea-level variations along the northwestern Tethyan margin during the Valanginian C-isotope excursion: mineralogical evidence from the Vocontian Basin (SE France). *Palaeogeography, Palaeoclimatology, Palaeoecology*, 302: 243-254.

Dunham R.J. (1962) - Classification of carbonate rocks according to depositional texture. In: Ham W.E. (Eds) - Classification of carbonate rocks: 108-121. AAPG Memoir 1.

Dupraz C. & Strasser A. (1999) - Microbialites and microencrusters in shallow coral bioherms (Middle to Late Oxfordian, Swiss Jura Mountains). *Facies*, 40: 101-129.

Embry A.F. & Klovan J.E. (1971) - A late Devonian reef tract on northeastern Banks Island. N.W.T. *Bulletin of Canadian Petroleum Geology,* 19: 730-781.

Erba E., Bartolini A. & Larson R.L. (2004) - Valanginian Weissert oceanic anoxic event. *Geology*, 32: 149-152.

Esteban M. & Pray L.C. (1983) - Pisoids and pisolite facies (Permian), Guadalupe Mountains, New Mexico and West Texas. In: Peryt M.T. - Coated grains: 503-537. Berlin, Heidelberg: Springer Berlin Heidelberg.

Falces-Delgado S., García-Martínez N., Giannetti A. & Baeza-Carratal J.F. (2022) - Reef-associated depositional environments in the lowermost Cretaceous facies (Berriasian) from the Eastern Prebetic domain (South-Iberian Palaeomargin, SE Spain). *Cretaceous Research*, 137: 105225.

Frakes L.A., Francis J.E. & Syktus J.I. (1992) - Climate modes of the Phanerozoic: The History of the Earth's Climate over the Past 600 Million Years. Cambridge University Press, 274 pp.

Flügel E. (2010) - Microfacies of carbonate rocks. Analysis, Interpretation and Application. 2nd Edition. Springer, Heidelberg, Dordrecht, London, New York, 984 pp.

Föllmi K.B. & Godet A. (2013) - Palaeoceanography of Lower Cretaceous Alpine platform carbonates. *Sedimentology*, 60: 131-151.

Föllmi K.B. (2012) - Early Cretaceous life, environment and anoxia. *Cretaceous Research*, 35: 230-257.

Föllmi K. B., Bodin S., Godet A., Linder P., & Van De Schootbrugge B. (2007) - Unlocking paleo-environmental information from Early Cretaceous shelf sediments in the Helvetic Alps: stratigraphy is the key! *Swiss journal of geosciences*, 100: 349-369.

Föllmi K.B., Weissert H., Bisping M. & Funk H. (1994) - Phosphogenesis, carbon isotope stratigraphy, and carbonate-platform evolution along the Lower Cretaceous northern Tethyan margin. *Geological Society of America Bulletin*, 106: 729-746.

Föllmi K.B., Godet A., Bodin S. & Linder P. (2006) - Interactions between environmental change and shallow-water carbonate build-up along the northern Tethyan margin and their impact on the early Cretaceous carbon isotope record. *Paleoceanography*, 21: 1-16.

Gawlick H.J. & Schlagintweit F. (2006) - Berriasian drowning of the Plassen carbonate platform at the type-locality and its bearing on the early Eoalpine orogenic dynamics in the Northern Calcareous Alps (Austria). *International Journal of Earth Sciences*, 95: 451-462.

Gillan D. & Ridder De Ch. (1997) - Morphology of ferric ironencrusted biofilm forming on the shell of a burrowing bivalve (Mollusca). *Aquatic Microbial Ecology*, 12: 1-10.

Godet A., Föllmi K.B., Spangenberg J.E., Bodin S., Vermeulen J., Adatte A., Bonvallet L. & Arnaud H. (2013) - Deciphering the message of Early Cretaceous drowning surfaces from the Helvetic Alps: what can be learnt from platform to basin correlations? *Sedimentology*, 60: 152-173.

Gonzalez-Donoso J.M., Linares D., Martin-Algarra A., Rebollo M., Serrano F. & Vera J.A. (1983) - Discontinuidades estratigraficas durante el Cretacico en el Penibetico (Cordillera Betica): *Estudios Geologica*: 39: 71-116.

Grădinaru M., Lazăr I., Bucur, I.I., Grădinaru E., Săsăran E., Ducea M.N. & Andrăşanu A. (2016) - The Valanginian history of the eastern part of the Getic Carbonate Platform (Southern Carpathians, Romania): evidence for emergence and drowning of the platform. *Cretaceous Research*, 66(1): 11-42.

Granier B.R. (2021) - *Bacinella*, a discrete type of Mesozoic calcimicrobial structure. *Carnets de Geologie,* 21(01): 1-25.

Grover G. & Read J.F. (1978) - Fenestral and associated vadose diagenetic fabrics of tidal flat carbonates, Middle Ordovician New Market Limestone, southwestern Virginia. *Journal of Sedimentary Research*, 48(2): 453-473.

Hallock P. & Schlager W. (1986) - Nutrient excess and the demise of coral reefs and carbonate platforms. *Palaios*, 389-398.

Hallam A. (1985) - A review of Mesozoic climates. *Journal of the Geological Society*, 142(3): 433-445.

Haq B.U. (2014) - Cretaceous eustasy revisited. *Global and Planetary Change*, 113: 44-58.

Henrich R., Hartmann M., Reitner J., Schäfer P., Freiwald A., Steinmentz S., Dietrich P. & Theide J. (1992) - Facies belts and communities of the Arctic Vesterisbanken Seamount (Central Greenland Sea). *Facies*, 27: 71-104.

Hesse R. (1988) - Diagenesis 13. Origin of chert: Diagenesis of biogenic siliceous sediments. *Geoscience Canada*, 15(3): 171-192.

Hesse R. (1989) - Silica diagenesis: origin of inorganic and replacement cherts. *Earth-Science Reviews*, 26(1): 253-284.

Hillgärtner H. (1998) - Discontinuity surface on the shallow-marine platform (Berriasian-Valanginian, France and Switzerland). *Journal of Sedimentary Research*, 68: 1093-1108.

Höfling R. & Scott R.W. (2002) - Early and mid-Cretaceous buildups. In: Kiessling W., Flügel E. & Golonka J. - Phanerozoic Reef Patterns. *SEPM Special Publications*, 72: 521- 548. 10.2110/pec.02.72.0521.

Hu X., Scott R.W., Cai Y., Wang C. & Melinte-Dobrinescu M.C. (2012) - Cretaceous oceanic red beds (CORBs): Different time scales and models of origin. *Earth-Science Reviews*, 115(4): 217-248.

Immenhauser A., Hillgärtner H. & Van Betum E. (2005) - Microbial-foraminiferal episodes in the Early Aptian of the southern Tethyan margin: ecological significance and possible relation to oceanic anoxic event 1a. *Sedimentology*, 52: 77-99.

Ivanova D. & Chatalov A. (2022) - New Stratigraphical and Sedimentological Data on the Lower Cretaceous Rocks in Section Kalotina, Western Bulgaria. *Proceedings of the Bulgarian Academy of Sciences*, 75, 12: 1785-1795.

Ivanova D. & Koleva-Rekalova E. (2004) - Agglutinated foraminifers in the framework of Southwestern Bulgarian palaeoenvironmental evolution during the Late Jurassic and Early Cretaceous. In: Bubık M. & Kaminski M.A. - Proc. 6th Int. Workshop on Agglutinated Foraminifera. *Grzybowski Foundation Special Publication*, 8: 217-227.

Ivanova D., Kolodziej B., Koleva-Rekalova E. & Roniewicz E. (2008) - Oxfordian to Valanginian palaeoenvironmental evolution on the western Moesian Carbonate Platform: a case study from SW Bulgaria. *Annales Societatis Geologorum Poloniae*, 78: 65-90.

Ivanova D., Stoykova K. & Lakova I. (2000) - New microfossil data on the age relationship between Slivnitsa and Salash Formations in Dragoman region, Western Bulgaria. *Comptes rendus de l'Académie bulgare des Sciences,* 53(4): 71-74.

Jach R. (2002) - Lower Jurassic spiculite series from the Križna Unit in the Western Tatra Mts, Western Carpathians, Poland. *Annales Societatis Geologorum Poloniae*, 72(2): 131-144.

James N.P. & Choquette P.W. (1984) - Diagenesis 9. Limestones-the meteoric diagenetic environment. *Geoscience Canada*, 11(4): 161-194.

James N.P. (1997) - The cool-water carbonate depositional realm. In: James N.P. & Clarke J.A.D. (Eds) - Cool-Water Carbonates: 1-20. *SEPM Special Publications,* 56. doi:10.2110/pec.97.56.0001.

Jankičević J. (1978) - Barremien et Aptien des parties moyennes des Carpatho-Balkanides dans la Serbie orientale au point de vue du developpement d'Urgonien. *Geološki anali Balkanskoga poluostrva*, 42: 103-194 [in Serbo-Croatian, French summary].

Jenkyns H.C. (1991) - Origin of red nodular limestones (Ammonitico Rosso, Knollenkalke) in the Mediterranean Jurassic: a diagenetic model. In: Pelagic Sediments: on Land and Under the Sea. *IAS Special Publication,* 1: 249-271.

Kaya M. & Altiner D. (2015) - Microencrusters from the Upper Jurassic – Lower Cretaceous İnaltı Formation (Central Pontides, Turkey): remarks on the development of reefal/peri-reefal facies. *Facies*, 61. 10.1007/s10347-015-0445-5.

Kenter J.A., Harris P.M.M. & Della Porta G. (2005) - Steep microbial boundstone-dominated platform margins–examples and implications. *Sedimentary Geology*, 178(1-2): 5-30.

Kiessling W., Flügel E. & Golonka J. (2003) - Patterns of Phanerozoic carbonate platform sedimentation. *Lethaia*, 36: 195-225.

Kolodziej B. & Ivanova D. (2021) - Microencruster-microbial-cement framework of the Upper Jurassic reef developed on the slope of the intra-Tethyan carbonate platform (Bulgaria). *Proceedings of the Geologists' Association*, 132.

Kräutner H.G. & Krstić B.P. (2003) - Geological map of the Carpatho-Balkanides between Mehadia, Oravita, Niš and Sofia. Geoinstitut, Belgrade.

Krstekanić N., Matenco L., Toljić M., Mandic O., Stojadinovic U. & Willingshofer E. (2020) - Understanding partitioning of deformation in highly arcuate orogenic systems: Inferences from the evolution of the Serbian Carpathians. *Global and Planetary Change*, 195: 103361.

Lackschewitz K.S., Grützmacher U. & Henrich R. (1991) - Paleoceanography and rotational block faulting in the Jurassic carbonate series of the Chiemgau Alps (Bavaria). *Facies*, 24: 1-24.

Lajoie J. & Chagnon A. (1973) - Origin of red beds in a Cambrian flysch sequence, Canadian Appalachians, Quebec. *Sedimentology*, 20(1): 91-103.

Larson R.L. & Erba E. (1999) - Onset of the Mid-Cretaceous greenhouse in the Barremian-Aptian: Igneous events and the biological, sedimentary, and geochemical responses. *Paleoceanography*, 14(6): 663-678.

Lazăr I., Grădinaru M. & Petrescu L. (2013) - Ferruginous microstromatolites related to Middle Jurassic condensed sequences and hardgrounds (Bucegi Mountains, Southern Carpathians, Romania). *Facies* 59(2): 359-390. doi:10.1007/s10347-012-0313-5

Leinfelder R.R., Nose M., Schmid D. & Werner M. (1993a) - Microbial crusts of the Late Jurassic: composition, palaeoecological significance and importance in reef construction. *Facies*, 29: 195-230.

Leinfelder R.R., Krautter M., Nose M., Ramalho M.M. & Werner W. (1993b) - Siliceous sponge facies from the Upper Jurassic of Portugal. *Neues Jahrbuch für Geologie und Paläontologie,* 189: 199-245.

Leinfelder R.R., Schlagintweit F., Werner W., Ebli O., Nose M., Schmid D.U. & Hughes G.W. (2005) - Significance of stromatoporoids in Jurassic reefs and carbonate platforms-concepts and implications. *Facies*, 51: 287-325.

Lohman K.C. (1988) - Geochemical patterns of meteoric diagenetic systems and their application to studies of paleokarst. In: James N.P. & Choquette P.W. (Eds) - Paleokarst: 58-80. New York, NY: Springer New York.

Longman M.W. (1980) - Carbonate diagenetic textures from nearsurface diagenetic environments. *AAPG bulletin*, 64(4): 461-487.

Mamet B. & Préat A. (2006) - Iron-bacterial mediation in Phanerozoic red limestones: state of the art. *Sedimentary Geology*, 185(3-4): 147-157.

Mandov G. & Nikolov T. (2001) - Stratigraphy of the Lower Cretaceous in the region between Dragoman and Kalotina villages, Sofia district (Western Bulgaria). *Annual of Sofia University "St. Kliment Ohridski" Faculty of Geology and Geography*, 91(1): 5-26 [in Bulgarian with English abstract].

Martinez M., Aguirre-Urreta B., Dera G., Lescano M., Omarini J., Tunik M., O'Dogherty L., Aguado R., Company M. & Bodin S. (2023) - Synchrony of carbon cycle fluctuations, volcanism and orbital forcing during the Early Cretaceous. *Earth-Science Reviews*, 239: 104356.

Masse J. P., Villeneuve M., Leonforte E. & Nizou J. (2009) - Block tilting of the North Provence early Cretaceous carbonate margin: stratigraphic, sedimentologic and tectonic data. *Bulletin de la Société géologique de France*, 180(2): 105-115.

Merino-Tomé O., Della Porta G., Kenter J.A.M., Verwer K.,

Harris P.M., Adams E., Playton T. & Corrochano D. (2012) - Sequence development in an isolated carbonate platform (Lower Jurassic, Djebel Bou Dahar, High Atlas, Morocco): influence of tectonics, eustacy and carbonate production. *Sedimentology* 59: 118-155.

Michalík J., Lintnerová O., Reháková D., Boorová D. & Šimo V. (2012) - Early Cretaceous sedimentary evolution of a pelagic basin margin (the Manín Unit, central Western Carpathians, Slovakia). *Cretaceous Research*, 38: 68-79.

Mircescu C. V., Bucur I. I. & Săsăran E. (2014) - Dasycladalean algae from Upper Jurassic–Lower Cretaceous limestones of Piatra Craiului Massif (South Carpathians, Romania) and their relationship to paleoenvironment. *Studia UBB Geologia*, 59(1), 5-27.

Mircescu C.V., Bucur I.I., Săsăran E., Pleş G., Ungureanu R. & Oprişa A. (2019) - Facies evolution of the Jurassic-Cretaceous transition in the Eastern Getic Carbonate Platform, Romania: Integration of sequence stratigraphy, biostratigraphy and isotope stratigraphy. *Cretaceous Research*, 99: 71-95.

Mircescu C.V., Bucur I.I. & Pleş G. (2022) - The Jurassic-Cretaceous transition in deep- and shallow water carbonate depositional settings: a case study from the easternmost Getic Carbonate Platform. *Facies*, 68: 5.

Morales C., Gardin S., Schnyder J., Spangenberg J., Arnaud-Vanneau A., Arnaud H., Adatte T. & Föllmi K. (2013) - Berriasian and early Valanginian environmental change along a transect from the Jura Platform to the Vocontian Basin. *Sedimentology*, 60: 36-63. 10.1111/sed.12019.

Morales C., Spangenberg J.E., Arnaud-Vanneau A., Adatte T. & Föllmi K.B. (2016) - Evolution of the northern Tethyan Helvetic Platform during the late Berriasian and early Valanginian. *The Depositional Record*, 2(1): 47-73.

Mullins H.T., Thompson J.B., McDougall K. & Vercoutere T.L. (1985) - Oxygen-minimum zone edge effects: evidence from the central California coastal upwelling system. *Geology*, 13(7): 491-494.

Nembrini M., Della Porta G. & Berra F. (2021) - Development of coral-sponge-microbialite reefs in a coated grain-dominated carbonate ramp (Upper Jurassic, eastern Sardinia, Italy). *Facies*, 67(1): 1-32. https://doi.org/10.1007/s10347-020-00616-7.

Obasi C.C., Terry D.O., Jr., Myer G.H. & Grandstaff D.E. (2011) - Glauconite composition and morphology, shocked quartz, and the origin of the Cretaceous(?) main fossiliferous layer (MFL) in Southern New Jersey, U.S.A. *Journal of Sedimentary Research*, 81: 479-494.

Patrulius D. (1976) - Upper Jurassic – Lower Cretaceous carbonate rocks in the eastern part of the Getic Carbonate Platform and the adjacent flysch troughs. In: Patrulius D., Draganescu A., Baltres A., Popescu B., Radan S. (Eds) - Carbonates Rocks and Evaporites-Guidebook: 71-82. International Colloquium on Carbonates Rocks and Evaporites, Guidebook Series 15. Institute of Geology and Geophysics, Bucharest.

Patrulius D. & Avram E. (1976) - Stratigraphie et correlations des terrains neocomiens et barremo-bedouliens du couloir de Dâmbovicioara (Carpathes Orientalşi). *Geofizică,* 52, 135-160.

Petrova S., Andreeva P., Metodiev L., Rehakova D., Jozef M. & Iskra L. (2017) - Calpionellid biostratigraphy and microfacies analysis of a Tithonian-Berriasian carbonate succession in the Western Srednogorie (Bulgaria). *Geologica Balcanica*, 46: 65-92.

Pleş G., Oprişa A., Bucur I.I., Săsăran E., Mircescu C.V., Oltean G. & Iacob R. (2019) - The central-western Getic Carbonate Platform: Upper Jurassic to Lower Cretaceous biostratigraphy and sedimentary evolution of the Cioclovina–Banita sector (Southern Carpathians, Romania). *Facies*, 65: 32.

Pleş G., Schlagintweit F., Kołodziej B., Bucur I.I., Gawlick H. J., Mircescu C.V., & Lazăr I. (2024) - Upper Jurassic–lowermost Cretaceous hybrid build-ups of the Western Tethys Realm: Cement-rich microencruster-microbialite-calcified sponge framework. *Palaeogeography, Palaeoclimatology, Palaeoecology*, 639: 112035.

Préat A., Mamet B., Bernard A. & Gillan D. (1999) - Bacterial meditation, red matrices diagenesis, Devonian, Montagne Noire (southern France). *Sedimentary Geology*, 126: 223 - 242.

Radoičić R. (1978) - On distribution of dasycladalean in the Lower Cretaceous of Kurilovo, East Serbia. *Bulletin du Museum d'Histoire naturelle Beograd*, Series A 33: 183-197 (in Serbio-Croatian, with English summary).

Ricci C., Rusciadelli G., Della Porta G., Lanfranchi A., Jadoul F. & Lathuilière B. (2018) - Sedimentary evolution of a coral-, microbialites-and debris-rich Upper Jurassic reef (upper Tithonian, eastern Sardinia, Italy). *Sedimentary Geology*, 376: 113-135.

Ritterbush K. (2019) - Sponge meadows and glass ramps: State shifts and regime change. *Palaeogeography, Palaeoclimatology, Palaeoecology*, 513: 116-131.

Roniewicz E. (2008) - Kimmeridgian-Valanginian reef corals from the Moesian platform from Bulgaria. *Annales Societatis Geologorum Poloniae*, 78(2): 91-134.

Ross D. & Skelton P.W. (1993) - Rudist formations of Cretaceous A palaeoecological, sedimentological and stratigraphical review. In: Wright V.P. (Eds) - Sedimentology Review, 1: 73-91. Oxford, UK, Blackwell Scientific Publications.

Săndulescu M. (1984) Geotectonica Romaniei. Editura Tehnica, Bucureşti, 334 pp.

Sapunov I., Tchoumatchenco P., Dodekova L. & Bakalova D. (1985) - Stratigraphy of the Callovian and Upper Jurassic rocks in Southwestern Bulgaria. *Geologica Balcanica*, 15: 3-61.

Schlager W. (1981) - The paradox of drowned reefs and carbonate platforms: *Geological Society of America Bulletin*, 92: 197-211.

Schlager W. (1989) - Drowning unconformities on carbonate platforms. In: Crevello P.D., Wilson J.L., Sarg J.F. & Read J.F. (Eds.) - Controls on Carbonate Platform and Basin Development. *SEPM, Special Publication,* 44: 15-25.

Schlager W. (1999a) - Scaling of sedimentation rates and drowning of reefs and carbonate platforms. *Geology*, 27(2): 183-186.

Schlager W. (1999b) - Type 3 Sequence Boundaries. In Advances in Carbonate Sequence Stratigraphy: Application to Reservoirs, Outcrops and Models. *SEPM* (*Society for Sedimentary Geology*) *Special Publication*, 63: 35-45.

Schlager W. (2000) - Sedimentation rates and growth potential of tropical, cool-water and mud-mound carbonate systems. In: Insalaco E., Skelton P.W. & Palmer T.J. (Eds) - Carbonate Platform Systems: Components and Interactions, *Geological Society, London, Special Publications*, 178: 217-227.

Schlager W. (2003) - Benthic carbonate factories of the Phanerozoic. *International Journal of Earth Sciences*, 92: 445-

464. doi:10.1007/s00531- 003-0327-x.

Schlager W. & Camber O. (1986) - Submarine slope angles, drowning unconformities, and self-erosion of limestone escarpments. *Geology*, 14(9): 762-765.

Schlagintweit F. (2012) - New insights into *Troglotella incrustans* Wernli & Fookes, 1992, a fascinating Upper Jurassic-Upper Cretaceous foraminifer, *Studia UBB Geologia,* 57(2): 17-26 doi: http://dx.doi.org/10.5038/1937-8602.57.2.2

Schlagintweit F. & Bucur I.I. (2023) - New records of late Berriasian and late Valanginian Orbitolinidae (Foraminifera) from the eastern Getic Carbonate Platform (South Carpathians, Romania). *Cretaceous Research*, 148: 105502.

Schlagintweit F. & Ebli O. (1999) - New results on microfacies, biostratigraphy and sedimentology of Late Jurassic-Early Cretaceous platform carbonates of the Northern Calcareous Alps Part I: Tressenstein Limestone, Plassen Formation. *Abhandlungen-Geologischen Bundesanstalt*, 56(2): 379-418.

Schlagintweit F. & Krajewski M. (2015) - *Sarmentofascis*? *digitatus* n. sp., a new cladocoropsid stromatoporoid from the Tithonian-early Berriasian (Late Jurassic – Early Cretaceous) of the Ay-Petri massif (Crimea Peninsula). *Neues Jahrbuch für Geologie und Palaontologie - Abhandlungen*, 277 (2): 141-151.

Schmid S.M., Bernoulli D., Fügenschuh B., Matenco L., Schefer S., Schuster R., Tischler M. & Ustaszewski K. (2008) - The Alpine–Carpathian–Dinaridic orogenic system: correlation and evolution of tectonic units. *The Swiss Journal of Geosciences*, 101: 139-183.

Schmid S.M., Fügenschuh B., Kounov A., Matenco L., Nievergelt P., Oberhansli R., Pleuger J., Schefer S., Schuster R., Tomljenović B., Ustaszewski K. & van Hinsbergen D.J.J. (2020) - Tectonic units of the Alpine collision zone between Eastern Alps and western Turkey. *Gondwana Research*, 78: 308-374.

Sequero L.C., Aurell M. & Bádenas B. (2020) - Oncoid distribution in the shallow domains of a Kimmeridgian carbonate ramp (Late Jurassic, NE Spain). *Sedimentary Geology*, 398: 1-20. 105585. 10.1016/j.sedgeo.2019.105585.

Stampfli G. & Hochard C. (2009) Plate tectonics of the Alpine realm. *Geological Society, London, Special Publications,* 327: 89-111.

Stampfli G.M. & Borel G.D. (2002) A plate tectonic model for the Paleozoic and Mesozoic constrained by dynamic plate boundaries and restored synthetic oceanic isochrons. *Earth and Planetary Science Letters Journal*, 196: 17-33.

Strasser A. (1986) - Ooids in Purbeck limestones (lowermost Cretaceous) of the Swiss and French Jura. *Sedimentology*, 33: 711-727.

Tucker M.E. & Wright V.P. (1990) - Carbonate Sedimentology. Wiley-Blackwell, Oxford, 482 pp.

Ungureanu R., Săsăran E., Bucur I.I., Ungur C.G. & Mircescu C.V. (2015) - The Berriasian-Valanginian and Aptian deposits from the north-western part of the Piatra Craiului Massif: Stratigraphic relationships, facies and depositional environments. *Acta Palaeontologica Romaniae*, 11(2): 59-74.

van Hinsbergen D., Schmid S., Maţenco L., Maffione M., Vissers R., Gürer D. & Spakman W. (2020) - Orogenic architecture of the Mediterranean region and kinematic reconstruction of its tectonic evolution since the Triassic. *Gondwana Research*, 81: 79-229.

Védrine S., Strasser A. & Hug W. (2007) - Oncoid growth and distribution controlled by sea-level fluctuations and climate (Late Oxfordian, Swiss Jura Mountains). *Facies*, 53: 535-552.

Veizer J., Ala D., Azmy K., Bruckschen P., Buhl D., Bruhn F., Carden G.A.F., Diener A., Ebneth S., Godderis Y., Jasper T., Korte C., Pawellek F., Podlaha O.G. & Strauss H. (1999) - $^{87}Sr/^{86}Sr$, $\delta^{13}C$ and $\delta^{18}O$ evolution of Phanerozoic seawater. *Chemical Geology*, 161: 59-88.

Verwer K., Della Porta G., Merino-Tomé O. & Kenter J.A.M. (2009) - Controls and predictability of carbonate facies architecture in a Lower Jurassic three-dimensional barrier-shoal complex (Djebel Bou Dahar, High Atlas, Morocco). *Sedimentology*, 56(6): 1801-1831.

Walter B. (1989) - Au Valanginien superieur, une crise de la faune de bryozoaires: indication d'un important refroidissement dans le Jura. *Palaeogeography, Palaeoclimatology, Palaeoecology*, 74: 255-263.

Weissert H. & Erba E. (2004) - Volcanism, CO_2 and palaeoclimate: a Late Jurassic – Early Cretaceous carbon and oxygen isotope record. *Journal of the Geological Society*, 161(4): 695-702.

Weissert H., Lini A., Föllmi K.B. & Kuhn O. (1998) - Correlation of Early Cretaceous carbon isotope stratigraphy and platform drowning events: a possible link? *Palaeogeography, Palaeoclimatology, Palaeoecology*, 137: 189-203.

Wright V.P. (1994) - Palaeosols in shallow marine carbonate sequences. *Earth-Science Reviews*, 35: 367-395.

Wright V.P. (2007) - Calcrete. In: Nash D.J., McLaren S.J. (Eds) - Geochemical Sediments and Landscapes, 10-45. Blackwell, Oxford.